Magnetic Structure and Spin Waves in the Kagomé Jarosite compound $KFe_3(SO_4)_2(OH)_6$

T. Yildirim,[1] and A. B. Harris,[2]
(1) NIST Center for Neutron Research, National Institute of Standards and Technology, Gaithersburg, Maryland 20899
(2) Department of Physics and Astronomy, University of Pennsylvania, Philadelphia, PA, 19104
(Dated: February 6, 2008)

We present a detailed study of the magnetic structure and spin waves in the Fe jarosite compound $KFe_3(SO_4)_2(OH)_6$ for the most general Hamiltonian involving one- and two-spin interactions which are allowed by symmetry. We compare the calculated spin-wave spectrum with the recent neutron scattering data of Matan *et al.* for various model Hamiltonians which include, in addition to isotropic Heisenberg exchange interactions between nearest (J_1) and next-nearest (J_2) neighbors, single ion anisotropy and Dzyaloshinskii-Moriya (DM) interactions. We concluded that DM interactions are the dominant anisotropic interaction, which not only fits all the splittings in the spin-wave spectrum but also reproduces the small canting of the spins out of the Kagomé plane. A brief discussion of how representation theory restricts the allowed magnetic structure is also given.

PACS numbers: 75.30.Ds,75.10.Jm, 75.50.Ee

I. INTRODUCTION

In search for unusual magnetic ground states and spin dynamics, frustrated systems have been the main focus of both theoretical and experimental investigations in recent years.[1,2,3,4,5,6,7,8,9,10] In frustrated magnetic systems,[1,2] the energies of the various spin interactions compete and therefore they can not be simultaneously minimized. This competition can be induced by the geometry of the lattice on which the spins are arranged, in which case the phenomenon is called *geometrical frustration* and it often leads to quite unusual low temperature spin structures and dynamics. The nearest neighbor (nn) Heisenberg antiferromagnet (AF) on the corner-sharing Kagomé lattice is one of the most studied systems since it has all the ingredients such as low dimensionality, strong frustration, and low coordination number, required for a disordered "spin liquid" ground state.[3,4,5,6,7,8]

Figure 1 shows three possible Néel states of the Kagomé lattice nn antiferromagnet. In the classical limit, all ground states satisfy the "120° structure", in which the angle between each nn pair of spins is 120°. Fig. 1a-b shows **q**=0 type ordering with respectively positive and negative chirality. For positive (negative) chirality the direction in which the spins rotate as one traverses clockwise the triangle of sites is clockwise (counterclockwise). Fig. 1c shows the $\sqrt{3}\times\sqrt{3}$ spin structure which has triangles with both positive and negative chirality. From the spin configurations shown in Fig. 1, it is clear the the classical ground state has a continuous degeneracy due to the "weathervane" rotation of the spins[3,4,5,6,7,8] and therefore no long range magnetic order is expected even at zero temperature. However, in real systems, there are small perturbations such as next nearest neighbor (nnn) interactions,[5] anisotropies or defects. It has been also shown that thermal or quantum fluctuations could also lift some of the continuous degeneracy known as "order by disorder," yielding coplanar spin structures.[9,10]

Despite the extensive theoretical studies that suggest many possible fascinating frustrated ground states for the Kagomé nn AF, few experimental realizations exist for the system. The initial experimental studies were focused on the layered garnet, $SrCr_xGa_{12-x}O_{19}$.[11,12] However the interpretation of the magnetic properties of this system were complicated by the presence of an additional triangular lattice interposed between Kagomé layers and by the inherent configurational randomness associated with the random alloying. In recent years, it has been shown that the jarosite family of miner-

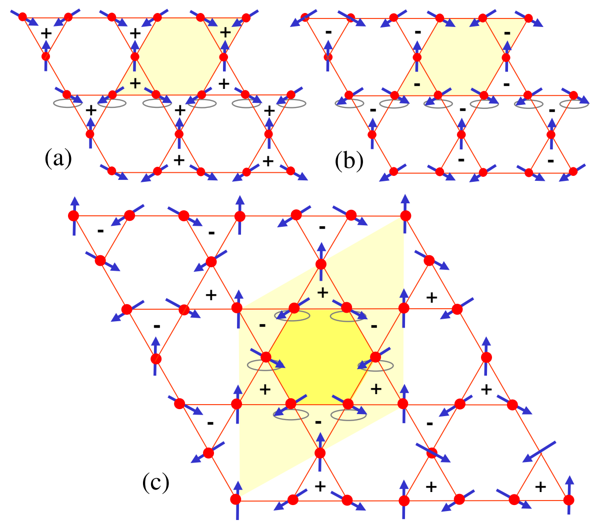

FIG. 1: (Color online) Three possible Néel states of the Kagomé lattice nn AF: (a) **q**=0 with positive chirality, (b) **q**=0 with negative chirality, and (c) $\sqrt{3}\times\sqrt{3}$ structure. The plus/minus signs indicate the chirality of spins on the elemental triangles. The shaded (yellow) areas indicate the magnetic unit cells. Note that the Néel sates shown above have continuous degeneracy as the spins on a line (a-b) and on a hexagon (c) can be rotated out of the plane as shown by ellipses without changing the classical ground state energy.

als $AM_3(OH)_6(SO_4)_2$,[13,14,15,16,17,18,19,20,21] (where A is monovalent ion such as K^+, and M is trivalent cation such as Fe^{3+}, Cr^{3+}, or V^{3+}) form much better realization of the two dimensional (2D) Kagomé lattice. As shown in Fig. 2 for M=Fe jarosite, the magnetic ion M^{3+} is centered in a slightly distorted and tilted oxygen octahedra, and it forms a Kagomé lattice in the ab-plane. The Kagomé planes are widely separated by nonmagnetic A^+ and SO_4^{-2} ions. With an exception of the hydronium jarosite $(H_3O)Fe_3(OH)_6(SO_4)_2$, all members of jarosite family are found to exhibit long range magnetic order (LRO) at finite temperatures with varying ground state spin configurations and exchange interaction strengths depending on the magnetic ion M. The strength of exchange interaction is the greatest for the parent M=Fe^{3+} ($d^5, L = 0, S = 5/2$) jarosite with Curie-Weiss temperature $\Theta_{CW} = -800$ K and $T_N \approx 65$ K. Replacement of the Fe^{3+} centers by Cr^{3+} ($d^3, S = 1/2$) also affords an antiferromanetically ordered material but with a significant reduced $\Theta_{CW} = -67$ K and $T_N \approx 2$ K. Interestingly, when the magnetic ion is replaced by V^{3+}, the ground state is changed to ferromagnetic Kagomé layers which are coupled antiferromanetically.[18] As we will discuss detail below, such a ferromagnetic ordering on the Kagomé lattice is allowed by the representation theory in contrast to a previous analysis.[15]

Among the members of the jarosite family, $KFe_3(OH)_6(SO_4)_2$ (FeJ) is probably the most studied one. The magnetic ground state of FeJ was first investigated by Townsend *et al.* using neutron diffraction.[13] However, later it became clear that the proposed spin configuration in Ref. 13 was not quite correct.[14] Inami *et al*[14] presented a detailed neutron scattering study and determined that the FeJ has 2D Kagomé planes with the **q**=0 spin-structure with positive chirality as shown in Fig. 1a. They observed that the unit cell along the c-axis is doubled in the magnetic phase, suggesting the the Kagomé planes are antiferromagnetically coupled. Field-dependent magnetization measurements[21] have suggested that each Kagomé plane has a small ferromagnetic component due to the canting of the spins in the **q**=0 structure with positive chirality (this is the so called "umbrella" configuration). However to the best of our knowledge, there is no experimental data which indicates the direction of this spin-canting whose determination would allow one to deduce the sign of some of the anisotropic terms in the Hamiltonian, as we will discuss in detail later.

The fact that FeJ exhibits LRO at finite temperature indicates that there are interactions other than nn isotropic AF superexchange, such as nnn interactions, anisotropies, etc. Inami *et al.*[14,16] have pointed out that in FeJ, the oxygen-octahedra are significantly tilted (see Fig. 2), thereby inducing a strong single-ion crystal field (CF) anisotropy. They used this CF term in the Hamiltonian to explain the observed spin configuration and to calculate the spin-wave spectrum. However in their spin-wave calculations, they neglected the canting of the spins out of the Kagomé plane. As we will discuss in detail below, this neglect leads to qualitatively wrong results for the spin-wave energy gaps at the high symmetry points in the Brillouin zone.

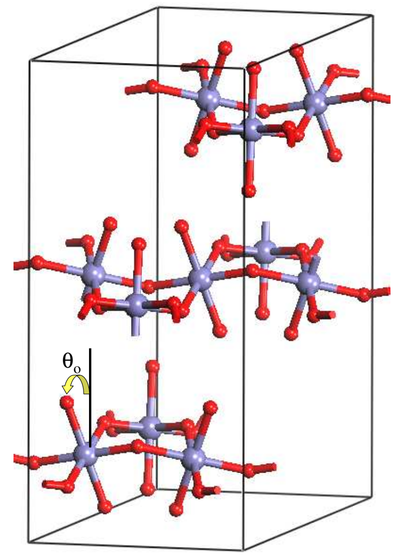

FIG. 2: (Color online) Conventional unit cell of FeJ. For clarity only Fe, big spheres (blue) and the octahedral oxygens, small spheres (red) are shown. The tilting angle, θ_o of the FeO_6 octahedra is also shown.

Elhajal *et al.*[20] have pointed out that CF terms in FeJ should be fairly small because they are second order in the spin-orbit coupling and Fe^{3+} has a spherical charge distribution (*i. e.* $L = 0$). Hence as an alternative source of anisotropy, they suggested that the Dzyaloshinskii-Moriya (DM) interaction of the form:[23,24] $D_{ij}S_i \times S_j$ could stabilize the experimentally observed spin structure. Indeed, the z-component of the DM vector (the definition of its components is given below) forces the spins to lie in the $ab-$plane and therefore effectively acts like an easy-plane anisotropy. The sign of D_z can distinguish between the **q**=0 states with negative and positive chirality. Since the $\sqrt{3} \times \sqrt{3}$ state has triangles with both positive and negative chirality, the D_z term alone will not affect the energy of this state. Furthermore if we introduce a D_y component, we break the rotational symmetry around the c-axis and create a small anisotropy with respect to in-plane orientations. The effect of D_y is also to cant the spins (so that they have a small out-of-plane component) into the observed "umbrella" spin configuration. Finally, since the DM interaction occurs at first-order in the spin-orbit coupling, it is expected to be larger than the CF terms of Inami *et al.*[14,16]

In order to identify the origin of the magnetic interactions that are responsible for the LRO in FeJ compounds, clearly we need more experimental data such as the observed spin-wave spectrum. Fortunately, thanks to the very recent progress in the synthesis of high-quality single crystals of FeJ compounds,[19,21] such spin-wave data

has been recently become available.[22] Here we present a detailed theory for the spin-wave spectrum in FeJ compound for generic nn and nnn superexchange interactions including the CF and DM terms discussed above. As we shall see below, the DM term along with the nn and nnn isotropic interactions can explain quite well not only the observed spin configuration but also the observed spin-wave spectrum.

Briefly this paper is organized as follows. In the next section we first discuss the symmetry of the FeJ structure in the paramagnetic phase and then present a brief representation analysis of the allowed magnetic structures. In doing so, we discovered that in Wills's analysis,[15] some of the ferromagnetic wavefunctions were missing. Indeed such a structure consisting of ferromagnetic easy-plane Kagomé planes has been observed for a NaV-jarosite.[18] In this section, we also argue that characterization by irreducible representations is more fundamental than by the chirality of the **q**=0 state. In Sec. III we discuss the generic magnetic Hamiltonian that we use in our calculations. In this section, we first discuss the symmetry of the Hamiltonian matrix and then its representation in a coordinate system in which the local z-axis coincides with the local direction of the spin moments. Here we also treat the canting of the spin orientations. In Sec. IV, we derive analytic results for the spin-wave energy gaps at the Γ, X and Y-points of the Brillouin zone. In Sec. V, we present spin-wave spectra from numerical calculations and compare the results with the recent spin-wave data of Matan *et al.*[22] Here we consider several models with increasing complexity. We find that the DM terms combined with nn and nnn isotropic exchange interactions give an excellent fit to the data. Our conclusions are summarized in Sec. VI. The details of the diagonalization of the spin Hamiltonian were given in Appendices. In Appendix A, we describe the transformation to the boson representations of the spins. In Appendix B, we discuss how to obtain the normal mode energies and eigenvectors. Appendix C describes the actual calculations of the matrix elements and Appendix D gives the results for the dynamical structure factor in terms of the normal mode energies and eigenvectors.

II. CRYSTAL AND MAGNETIC STRUCTURE

A. Symmetry of the Paramagnetic Phase

We first discuss the symmetry of the paramagnetic phase. In Fig. 2 we show the conventional unit cell which contains three formula units of FeJ. The primitive unit cell (which contains one formula unit of FeJ) is rhombohedral, with basis lattice vectors

$$\begin{aligned}
\mathbf{a}_1 &= (a/2)\hat{i} + (\sqrt{3}a/6)\hat{j} + (c/3)\hat{k} \ , \\
\mathbf{a}_2 &= -(a/2)\hat{i} + (\sqrt{3}a/6)\hat{j} + (c/3)\hat{k} \ , \\
\mathbf{a}_3 &= -(\sqrt{3}a/3)\hat{j} + (c/3)\hat{k} \ , \qquad (1)
\end{aligned}$$

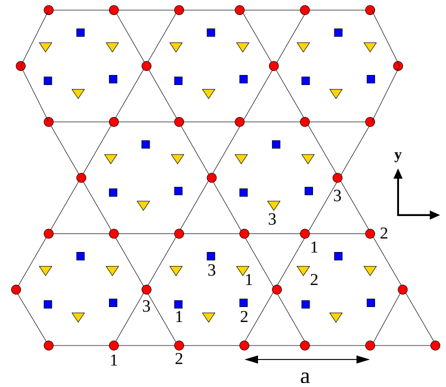

FIG. 3: (Color online.) Kagomé planes. The filled circles are x-y planes at $z = 0$, the filled squares are x-y planes at $z = c/3$, and the filled triangles are x-y planes at $z = 2c/3$. The positive z-axis is out of the plane. Representative sublattice numbers τ are given.

where c denotes the height of the conventional unit cell of Fig. 2. The space group of FeJ is R$\bar{3}$m, which is #166 in the International Tables of Crystallography.[25] In order to understand the magnetic properties of FeJ we show in Fig. 3 only the Fe $S = 5/2$ spins. Their locations within the primitive unit cell, denoted $\boldsymbol{\tau}_n$, are

$$\begin{aligned}
\boldsymbol{\tau}_1 &= (0,0,0) \ , \quad \boldsymbol{\tau}_2 = (a/2,0,0) \ , \\
\boldsymbol{\tau}_3 &= (a/4, a\sqrt{3}/4, 0) \ , \qquad (2)
\end{aligned}$$

where the components are given with respect to the orthogonal axes of Fig. 3. Notice that each plane (e. g. the filled circles) forms a Kagomé plane lattice. As one moves from one plane to the adjacent plane at more positive z, the Kagomé lattice is translated by $(a/2)\hat{i}+(\sqrt{3}a/6)\hat{j}$, or, equivalently by either $(-a/2)\hat{i}+(\sqrt{3}a/6)\hat{j}$ or $-(a\sqrt{3}/3)\hat{j}$.

Apart from translations the generators of the space group may be taken to be $\mathcal{I}$, spatial inversion about the center of a hexagon, r, a two-fold rotation about an axis parallel to the x-axis and passing through the center of the hexagon, and R, a three-fold rotation about an axis passing through the center of the hexagon perpendicular to the Kagomé plane. Since the center of a hexagon in one plane lies just above a triangle in an adjacent plane, the three-fold axis can be taken at the center of a triangle. The above operations imply the existence of mirror planes perpendicular to the Kagomé plane and bisecting the sides of the hexagons.

The reciprocal lattice basis vectors $\mathbf{b}_i$, which satisfy $\mathbf{a}_i \cdot \mathbf{b}_j = 2\pi\delta_{i,j}$, where $\delta_{i,j}$ is the Kronecker delta, are

$$\begin{aligned}
\mathbf{b}_1/(2\pi) &= (1/a)\hat{i} + (1/\sqrt{3}a)\hat{j} + (1/c)\hat{k} \\
\mathbf{b}_2/(2\pi) &= -(1/a)\hat{i} + (1/\sqrt{3}a)\hat{j} + (1/c)\hat{k} \\
\mathbf{b}_3/(2\pi) &= -(2/\sqrt{3}a)\hat{j} + (1/c)\hat{k} \ . \qquad (3)
\end{aligned}$$

Since interactions between adjacent Kagomé planes are very small, we may approximately describe the structure

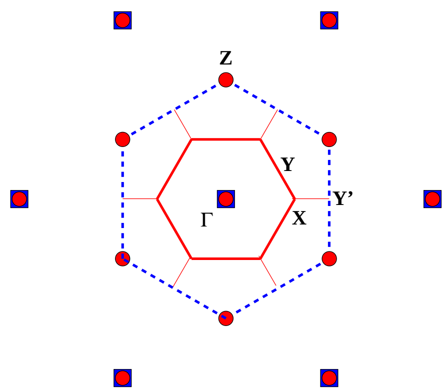

FIG. 4: (Color online.) Reciprocal lattices for the FeJ system (blue squares) and for the two-dimensional hexagonal lattice (red circles). The first Brillouin zone for the two-dimensional hexagonal system is indicated by heavy solid lines in red and that (in the $z = 0$ plane) for the FeJ system by heavy dashed lines in blue. The light solid lines in red mark the boundaries of neighboring hexagonal zones. The FeJ Brillouin zone is three times as large as the hexagonal zone.

in terms of a two-dimensional hexagonal lattice with basis vectors, $\mathbf{A}_i$, given by

$$\begin{aligned} \mathbf{A}_1 &= \mathbf{a}_1 - \mathbf{a}_2 = a\hat{i} \ , \\ \mathbf{A}_2 &= \mathbf{a}_2 - \mathbf{a}_3 = -(a/2)\hat{i} + (\sqrt{3}a/2)\hat{j} \ . \end{aligned} \quad (4)$$

The associated reciprocal lattice of this hexagonal lattice has basis vectors

$$\begin{aligned} \mathbf{B}_1/(2\pi) &= (1/a)\hat{i} + (1/\sqrt{3}a)\hat{j} \ , \\ \mathbf{B}_2/(2\pi) &= (2/\sqrt{3}a)\hat{j} \ . \end{aligned} \quad (5)$$

In contrast the three-dimensional reciprocal lattice vectors in the $z = 0$ plane for FeJ are

$$\begin{aligned} \mathbf{b}_1 - \mathbf{b}_2 &= (4\pi/a)\hat{i} \\ \mathbf{b}_2 - \mathbf{b}_3 &= -(2\pi/a)\hat{i} + (2\pi\sqrt{3}/a)\hat{j} \ . \end{aligned} \quad (6)$$

As shown in Fig. 4, the vectors of Eq. (5) define the hexagonal Brillouin zones and those of Eq. (6) define the boundaries of the FeJ Brillouin zone in the $z = 0$ plane. The first Brillouin zone of the FeJ system in the hexagonal plane has an area three times that of the two-dimensional hexagonal system. If there were absolutely no interactions between Kagomé planes, the spin-wave dispersion relation in the region in the first Brillouin zone of the FeJ system but outside that of the two-dimensional hexagonal system could be mapped into the dispersion relation inside the first Brillouin zone of the two-dimensional system and in this paper we adopt this picture. For the two dimensional system, spin-wave energies at points just outside the hexagonal Brillouin zone near point Y are exactly the same as at the corresponding point just inside the zone near Y. For the three dimensional FeJ system this is only approximately true. The spectra of these two points will differ due to interplanar interactions. Similarly, for the two-dimensional system the spin-wave energies at point Z are identical to those at Γ, whereas for the FeJ system they will differ due to interplanar interactions. We will show the spin-wave spectrum observed by Matan et al.[22] along the line $\Gamma - X - Y'$, where Y' is equivalent to Y if interplanar interactions are neglected.

B. Results of Representation Theory

A continuous phase transition may be described by a Landau expansion in powers of $\mathbf{S}_\tau(\mathbf{q})$, the Fourier components of the spin order parameters which are defined as

$$\mathbf{S}_\tau(\mathbf{q}) \ = \ (1\sqrt{N_{\rm uc}})\sum_{\mathbf{R}} \langle \mathbf{S}(\mathbf{R}+\boldsymbol{\tau})\rangle e^{i\mathbf{q}\cdot(\mathbf{R}+\boldsymbol{\tau})} \ , \quad (7)$$

where $\mathbf{S}(\mathbf{R}+\boldsymbol{\tau})$ is the spin at site τ in the unit cell at $\mathbf{R}$, $\langle\ \rangle$ denotes a thermal average, and $\mathbf{q}$ is the wavevector of the ordering. At quadratic order the Landau expansion for the free energy, F, assumes the form

$$F \ = \ \sum_{\tau,\tau';\alpha,\alpha'} c_{\tau,\alpha;\tau',\alpha'}(\mathbf{q}) S_{\tau,\alpha}(\mathbf{q}) S_{\tau',\alpha'}(-\mathbf{q}) \ , \quad (8)$$

where α labels Cartesian components and $S_{\tau,\alpha}(-\mathbf{q}) = S_{\tau,\alpha}(\mathbf{q})^*$. The ordering that actually occurs corresponds to the eigenvector associated with that eigenvalue of the quadratic form of Eq. (8) which first becomes negative (unstable) as the temperature is lowered starting from the paramagnetic phase. In view of the invariance of F with respect to the symmetry operations of the crystal, one can say that the eigenvectors give rise to an irreducible representation (irrep) of the space group of the crystal.[26] This analysis is straightforward and has been given previously,[15] although the results we present below seem to contradict that reference.

Because spin is a pseudovector, spatial inversion takes a spin into its spatially inverted location but does not reorient the spin. Since all spins are located at centers of inversion symmetry, we only need to consider irreps which are invariant under spatial inversion, and we denote these by Γ_n^+, where the label n assumes the values $1, 2, 3$ and the superscript indicates invariance under spatial inversion. For the one dimensional irreps (Γ_1^+ and Γ_2^+) the situation is quite simple: each eigenvector of F is also an eigenvector of each operation of the space group. Thus we show in Fig. 5 the possible spin configurations which correspond to one dimensional irreps. The actual spin configuration associated with irrep Γ_2^+ is a linear combination of the two configurations shown.

For the two dimensional irrep Γ_3^+ the situation is more complicated. Here one has p wavefunctions $\psi_j^{(3,1)}$, for $j = 1, 2, \ldots p$ which transform as the first row of the matrix representation of Γ_3^+ and their p partners $\psi_j^{(3,2)}$

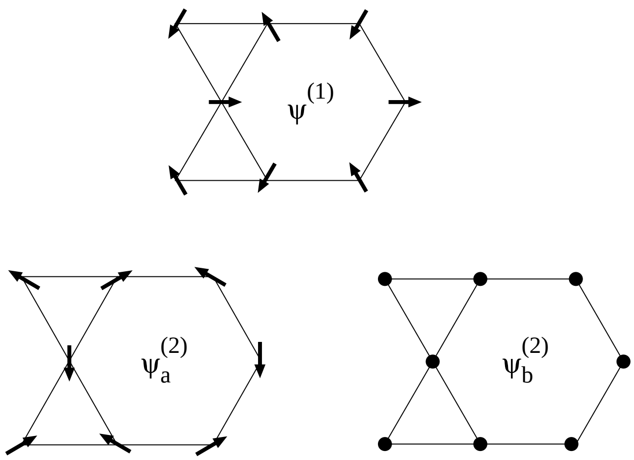

FIG. 5: Spin configurations which transform according to one dimensional irreps. Solid circles indicate spins pointing out of the page. Top: a configuration of Γ_1^+ for which the eigenvalue of r is $+1$ and R is $+1$. Bottom: two configurations for Γ_2^+ for which the eigenvalue of r is -1 and R is $+1$.

which transform as the second row of the matrix representation of Γ_3^+, where for FeJ $p = 3$.[15] We show these wavefunctions in Fig. 6. To be specific, if $\mathcal{O}$ is a symmetry operation and $\mathcal{M}(\mathcal{O})$ is a matrix representation of it according to Γ_3^+, then we have

$$\mathcal{O}\psi_j^{(3,n)} = \sum_m \mathcal{M}_{n,m}(\mathcal{O})\psi_j^{(3,m)} \ . \tag{9}$$

These wavefunctions of Γ_3^+ correspond to the choice

$$\mathcal{M}(r) \ = \ \begin{bmatrix} -1 & 0 \\ 0 & 1 \end{bmatrix} \ , \quad \mathcal{M}(R) = \begin{bmatrix} -1/2 & -\sqrt{3}/2 \\ \sqrt{3}/2 & -1/2 \end{bmatrix} \tag{10}$$

One can check that the wavefunctions shown in Fig. 6 actually do satisfy Eq. (9). Of course, all the wavefunctions shown here are orthogonal to one another and span the original subspace of spin components. (That appears not to be the case with the results of Ref. 15. In addition, his states do not seem to allow the net moment for a single Kagomé layer to lie in the Kagomé plane. Since this does happens for a Na jarosite,[18] the statement that the structure of the chromate jarosite must be the umbrella structure is not justified.)

C. Discussion of Results: Dipolar Interactions, Chirality

We now discuss the implications of the above results. The above results hold for two separate cases: in the ferromagnetic case, all Kagomé planes have the same spin structure (apart from a translation), whereas in the antiferromagnetic case successive Kagomé plane have their spins inverted. The ferromagnetic case corresponds to

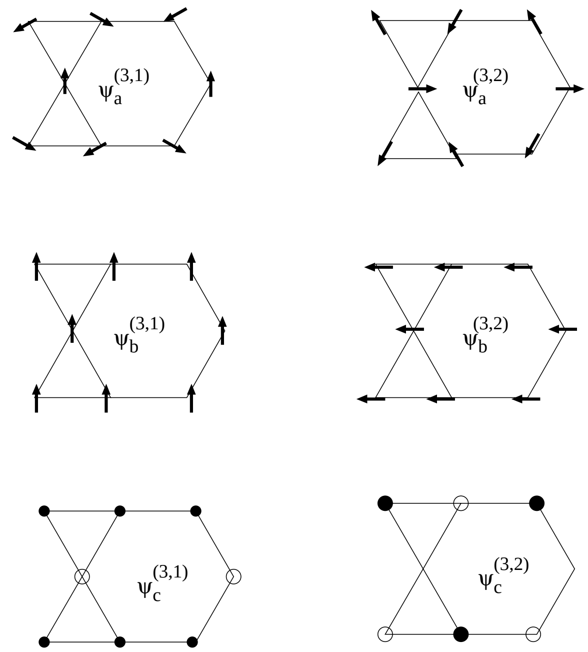

FIG. 6: Spin configurations which transform according to two dimensional irrep Γ_3^+. In the left (right) column we give the wavefunctions which transform according to the first (second) row of the matrices of the irrep. Arrows represent spins of unit length. Solid (open) circles indicate spins pointing perpendicularly into (out of) the Kagomé plane. For $\Psi_c^{(3,1)}$ the magnitudes of the inward spins are both equal to half that of the outward spin which is set to be $\sqrt{2}$. For $\Psi_c^{(3,2)}$ the nonzero magnitudes of the spins are both $\sqrt{3/2}$.

wavevector $\mathbf{q} = 0$, whereas the antiferromagnetic case corresponds to $\mathbf{q} = (3\pi/c)\hat{k}$.[15] Note that irrep Γ_2^+ has two wavefunctions. This means that any such structure generically consists of a linear combination of a ferromagnetic state (in a layer) with spins perpendicular to the plane and some in-plane ordering as well. This is the so-called "umbrella" state. The implication is that if one has an easy axis ferromagnet with spins perpendicular to the Kagomé plane, one unavoidably will have some in-plane order. Conversely, in the case of FeJ one has order of irrep Γ_3^+ in each plane which must be accompanied by a net out-of plane moment.

Note that the irreps Γ_1^+ and Γ_2^+ are Ising-like in that within these representations one can not uniformly rotate the spins. Thus the excitation spectrum must have a significant energy gap. In contrast irrep Γ_3^+ is x-y-like. One spin structure is some linear combination of the wavefunctions of the left column of Fig. 6. Alternatively, the free energy is unchanged if one instead takes the *same* linear combination of the wavefunctions of the right column of Fig. 6. The actual wavefunction is therefore characterized by four constants, α, β, γ and θ:

$$\psi \ = \ \cos\theta \left[\alpha\psi_a^{(3,1)} + \beta\psi_b^{(3,1)} + \gamma\psi_c^{(3,1)}\right]$$

$$+\sin\theta\left[\alpha\psi_a^{(3,2)}+\beta\psi_b^{(3,2)}+\gamma\psi_c^{(3,2)}\right] \ , \quad (11)$$

which can not be fixed by symmetry. At quadratic level in the Landau expansion, the free energy does not depend on θ and one would expect a Goldstone (gapless) mode. However, due to the discrete symmetry of the Kagomé plane, the anisotropy energy, F_A, which at lowest order is

$$E_A \ = \ K\cos(6\theta) \ , \quad (12)$$

will lead to a gap. If $K > 0$, the system will favor $\theta = \pi/6$ (or equivalent angles) whereas if $K < 0$ the system will favor angles equivalent to $\theta = 0$. Quadratic energies, such as the dipolar energy, will not lead to a gap. Accordingly, it is not surprising that we found that for Γ_3^+ the dipolar energy of the system was independent of θ.

It is interesting to note that if one assumes isotropic nearest neighbor (nn) and next-nearest neighbor (nnn) interactions, then spin configurations $\Psi^{(1)}$ and $\Psi_a^{(2)}$ have the same energy. However, in general irrep Γ^{2+} will have lower energy because it can accommodate a distortion into the configuration $\Psi_b^{(2)}$. In principle, local single-ion anisotropy[14] and/or DM interactions[20] can select a ground state from among these functions.

In the literature, there are frequent references to "chirality." Configurations have positive chirality, if when one traverses a triangle of spins clockwise, the spins rotate clockwise by $\Delta\phi = 120^{\mathrm{o}}$, whereas for negative chirality $\Delta\phi = -120^{\mathrm{o}}$. In our opinion, the characterization by irreps is more fundamental. One sees that the wavefunction of irrep Γ_1^+ and one of those of Γ_2^+ correspond to positive chirality and two of the wavefunctions for Γ_3^+ correspond to negative chirality. However, the sign of the chirality, of itself, does not indicate the presence or not of a gap in the excitation spectrum. Nor does the sign of the chirality correlate in an obvious way with the nature of other wavefunctions which may be admixed.

D. Actual Magnetic Structure

The actual magnetic structure[14] of FeJ is that shown in Fig. 7 associated with the wavevector $\mathbf{q} = 3\pi/c$. This means that successive Kagomé planes are translated (as they would be in the paramagnetic phase), but then in successive planes the spin orientations are reversed. This causes a doubling of the unit cell because after three translations, the sites are back to their original positions, but the spin orientations are reversed. Thus the magnetic unit cell contains twice as many layers as in the paramagnetic phase. Although each layer individually has a small ferromagnetic moment perpendicular to the Kagomé plane, the sign of this moment alternates in sign from one Kagomé net to the next, so that the sample exhibits no overall net moment. However, as in La_2CuO_4,[27] one has a spin-flop transition[21] when a magnetic field perpendicular to the Kagomé plane rearranges the planes so that their ferromagnetic moments are parallel.

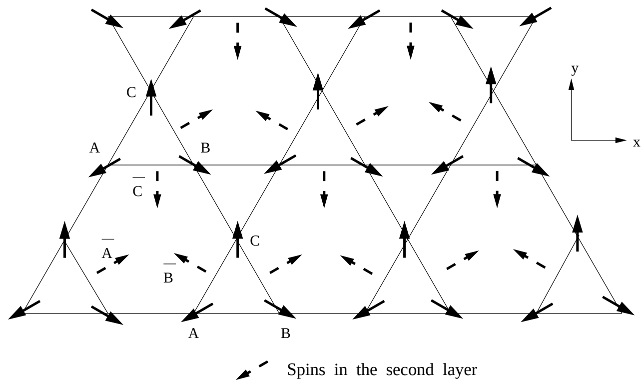

FIG. 7: Spin structure of FeJ as determined in Refs. 16, 14, and 21.

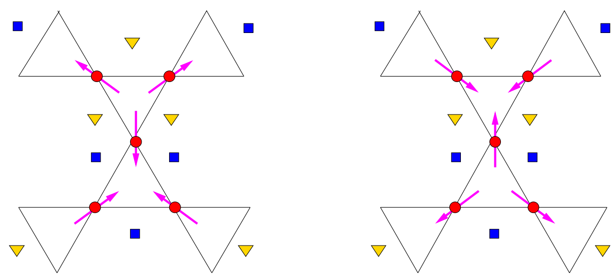

FIG. 8: (Color online) Spin structure of FeJ. The squares (blue) are sites in the Kagomé plane at $z = c/3$, the triangles (yellow) are sites in the plane at $z = -c/3$ and the circles (red) are sites in the plane at $z = 0$. The two symmetry related choices for spin orientations in the ordered phase are shown in the two panels.

Here we discuss some aspects of broken symmetry. One could ask whether the direction of the net moment of a Kagomé plane is fixed by interactions within the plane or is accidentally selected. First, we should note that if we had a single isolated Kagomé plane, then the two orientations or the net moment perpendicular to the plane would have identical free energy. As we will see, the direction of the net moment is fixed by the sign of the DM interaction. If we had a single Kagomé plane, such an interaction would not be allowed. So, the uniqueness of the direction of the moment perpendicular to the plane, must depend on the details of the three-dimensional structure and, because $+z$ and $-z$ are equivalent in the paramagnetic crystal, on the in-plane magnetic ordering. To see how this is possible consider Fig. 8. The actual spin structure is shown in the two panels of Fig. 8. The selection of one of these states is arbitrary and represents an example of broken symmetry. Let us see how the direction of the net moment perpendicular to the plane is fixed relative to the in-plane ordering. Suppose we have the broken symmetry selection of the structure shown in the left panel. There one sees that the in-plane spin moments point away from sites in the $z = -c/3$ plane and towards

sites in the $z = c/3$ plane. This indicates that positive and negative z are not equivalent *due to the presence of long-range magnetic order in the three-dimensional crystal structure*. This means that when the spin order is as in the left panel, the free energy will select the direction of the perpendicular moment. When the spin order is as in the right panel, the perpendicular moment will be reversed relative to what it was in the left panel. As we will see, when the in-plane order is selected, the direction of the out-of plane moment is determined by the sign of the y-component of the DM vector. It is interesting to note that the direction of the perpendicular moment can not be related to chirality. The structures shown in Fig. 8 have positive chirality whether seen by a viewer from in front of the page or behind the page. So associating a direction with chirality can not distinguish between directions into or out of the page.

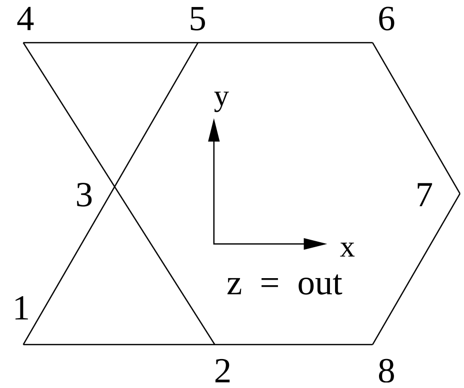

FIG. 9: Numbering of sites used to define nn and nnn interactions. The axes fixed in the crystal are shown.

III. MODEL HAMILTONIANS

A. General Hamiltonian

We neglect interactions between adjacent Kagomé planes. Accordingly, we now discuss the Hamiltonian of a single Kagomé plane. We first parameterize the nn interaction between spins #1 and #2 in Fig. 9, which we write as

$$\mathcal{H}_{12} \;=\; \sum_{\alpha\beta} M_{1,2}^{\alpha,\beta} \mathcal{S}_1^\alpha \mathcal{S}_2^\beta \;, \tag{13}$$

where the Greek superscripts label Cartesian components. The effect of the mirror plane perpendicularly bisecting the 1-2 bond is to change the sign of the y- and z-components of spin and simultaneously interchange spin labels. Thus taking the transpose of the matrix and changing the signs of the y- and z-components must leave the matrix invariant. So the interaction matrix must be of the form

$$\mathbf{M}_{1,2} \;\equiv\; \mathbf{M}^{(1)} = \begin{bmatrix} J_{xx}^{(1)} & D_z^{(1)} & -D_y^{(1)} \\ -D_z^{(1)} & J_{yy}^{(1)} & J_{yz}^{(1)} \\ D_y^{(1)} & J_{yz}^{(1)} & J_{zz}^{(1)} \end{bmatrix} \;, \tag{14}$$

where the superscript indicates an nn interaction and we introduce symmetric anisotropic exchange tensor $\mathbf{J}$ and antisymmetric DM interactions,[23,24] characterized by a DM vector $\mathbf{D}$. Note that the definition of Eq. (13) implies that

$$\mathbf{M}_{i,j} = \tilde{\mathbf{M}}_{j,i} \tag{15}$$

independent of what the local symmetry may be, where tilde indicates a transposed matrix.

We next characterize the nnn interaction between sites #5 and #2 in Fig. 9. This interaction has to be invariant under the two-fold rotation about the x-axis passing through the center of the bond. So the interaction matrix in Cartesian coordinates must be of the form

$$\mathbf{M}_{5,2} \;\equiv\; \mathbf{M}^{(2)} = \begin{bmatrix} J_{xx}^{(2)} & D_z^{(2)} & -D_y^{(2)} \\ -D_z^{(2)} & J_{yy}^{(2)} & J_{yz}^{(2)} \\ D_y^{(2)} & J_{yz}^{(2)} & J_{zz}^{(2)} \end{bmatrix} \;, \tag{16}$$

where $\mathbf{D}^{(2)}$ is the nnn DM interaction and $\mathbf{J}^{(2)}$ is the symmetric nnn interaction.

We also include a single-ion anisotropy energy $E_i^{(A)}$ for site i of the form

$$E_i^{(A)} \;=\; (1/2) \sum_{\alpha\beta} [\mathbf{C}']_i^{\alpha\beta} [S_i^\alpha S_i^\beta + S_i^\beta S_i^\alpha] \;. \tag{17}$$

The mirror x-plane through site #3 implies that the single-ion anisotropy matrix for this site is

$$\mathbf{C}'_3 \;=\; \begin{bmatrix} C'_{xx} & 0 & 0 \\ 0 & C'_{yy} & C'_{yz} \\ 0 & C'_{yz} & C'_{zz} \end{bmatrix} \;. \tag{18}$$

B. Transformation to Local Uncanted Axes

A direct, but inefficient, procedure would be to use the symmetry of the crystal to express all the other nn and nnn interactions in terms of the matrices of Eqs. (14) and (16), respectively. Instead, we proceed as follows. We express the nn and nnn interactions in terms of local axes which facilitate a spin-wave expansion. These local axes are defined so that the local positive z axis coincides with the projection of the local spin moment onto the Kagomé plane. These axes are illustrated in Fig. 10. The rotation matrices to transform to these local axes are

$$\mathcal{R}(\tau_1) \;=\; \begin{bmatrix} \frac{1}{2} & 0 & -\frac{\sqrt{3}}{2} \\ -\frac{\sqrt{3}}{2} & 0 & -\frac{1}{2} \\ 0 & 1 & 0 \end{bmatrix} \;,$$

$$\mathcal{R}(\tau_2) \ = \ \begin{bmatrix} \frac{1}{2} & 0 & \frac{\sqrt{3}}{2} \\ \frac{\sqrt{3}}{2} & 0 & -\frac{1}{2} \\ 0 & 1 & 0 \end{bmatrix} ,$$

$$\mathcal{R}(\tau_3) \ = \ \begin{bmatrix} -1 & 0 & 0 \\ 0 & 0 & 1 \\ 0 & 1 & 0 \end{bmatrix} . \tag{19}$$

The transformed interaction matrices, denoted $\mathcal{I}$, are such that

$$\mathcal{H}_{12} \ = \ \sum_{\alpha\beta} \mathcal{I}_{1,2}^{(\alpha,\beta)} S_1^\alpha S_2^\beta , \tag{20}$$

and

$$\mathcal{H}_{52} \ = \ \sum_{\alpha\beta} \mathcal{I}_{5,2}^{(\alpha,\beta)} S_5^\alpha S_2^\beta , \tag{21}$$

where now the spin components are taken in the local axes of Fig. 10 so that

$$\begin{aligned} \mathcal{I}_{1,2} \ &= \ \tilde{\mathcal{R}}(\tau_1)\mathbf{M}_{1,2}\mathcal{R}(\tau_2) \equiv \mathcal{I}^{(1)} \\ \mathcal{I}_{5,2} \ &= \ \tilde{\mathcal{R}}(\tau_1)\mathbf{M}_{5,2}\mathcal{R}(\tau_2) \equiv \mathcal{I}^{(2)} . \end{aligned} \tag{22}$$

Here

$$\mathcal{I}^{(n)} \ = \ \begin{bmatrix} -E_x^{(n)} & d_z^{(n)} & -d_y^{(n)} \\ -d_z^{(n)} & -E_y^{(n)} & E_{yz}^{(n)} \\ d_y^{(n)} & E_{yz}^{(n)} & -E_z^{(n)} \end{bmatrix} , \tag{23}$$

where

$$\begin{aligned} E_x^{(n)} \ &= \ \frac{3}{4}J_{yy}^{(n)} - \frac{1}{4}J_{xx}^{(n)} - \frac{\sqrt{3}}{2}D_z^{(n)} \\ &\equiv \ \frac{1}{2}J_n - \frac{\sqrt{3}}{2}D_z^{(n)} - \frac{7}{24}\Delta_n - \frac{1}{8}\eta_n \\ E_y^{(n)} \ &= \ -J_{zz}^{(n)} \\ &\equiv \ -J_n - \frac{1}{6}\Delta_n + \frac{1}{2}\eta_n \\ E_z^{(n)} \ &= \ \frac{3}{4}J_{xx}^{(n)} - \frac{1}{4}J_{yy}^{(n)} - \frac{\sqrt{3}}{2}D_z^{(n)} \\ &\equiv \ \frac{1}{2}J_n - \frac{\sqrt{3}}{2}D_z^{(n)} + \frac{5}{24}\Delta_n + \frac{3}{8}\eta_n \\ d_z^{(n)} \ &= \ -\frac{1}{2}D_y^{(n)} - \frac{\sqrt{3}}{2}J_{yz}^{(n)} \\ E_{yz}^{(n)} \ &= \ \frac{\sqrt{3}}{2}D_y^{(n)} - \frac{1}{2}J_{yz}^{(n)} \\ d_y^{(n)} \ &= \ -\frac{\sqrt{3}}{4}(J_{xx}^{(n)} + J_{yy}^{(n)}) - \frac{1}{2}D_z^{(n)} \\ &\equiv \ -\frac{\sqrt{3}}{2}J_n - \frac{1}{2}D_z^{(n)} + \frac{\sqrt{3}}{4}\left(\frac{\Delta_n}{6} - \frac{\eta_n}{2}\right) , \end{aligned} \tag{24}$$

where

$$\begin{aligned} J_n \ &= \ (J_{xx}^{(n)} + J_{yy}^{(n)} + J_{zz}^{(n)})/3 \\ \Delta_n \ &= \ J_{xx}^{(n)} + J_{zz}^{(n)} - 2J_{yy}^{(n)} , \quad \eta_n = J_{xx}^{(n)} - J_{zz}^{(n)} , \end{aligned} \tag{25}$$

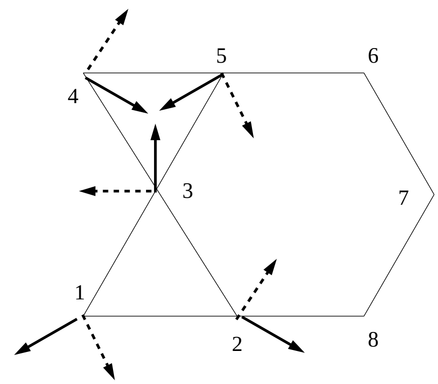

FIG. 10: Local axes of various sites. The local z-axis (indicated by the full line with arrow) is along the projection of the direction of the local magnetization onto the Kagomé plane. The local y-axis is perpendicularly out of the Kagomé plane. The local x-axis is in the Kagomé plane and is indicated by the dashed line with arrow.

so that J_n is the isotropic part of the nth neighbor interaction and we will only keep the anisotropic nn interactions, so that henceforth $\Delta_J \equiv \Delta_1$ and $\eta_J \equiv \eta_1$. We define $E_\alpha^{(n)}$ with a sign so that the interactions appear ferromagnetic in the local frame. The matrix elements $E_{yz}^{(n)}$ lead to a canted spin structure exhibiting weak ferromagnetism, as we will see in the next subsection. The single-ion anisotropy in the local frame can be written as

$$\mathbf{C} \ = \ \begin{bmatrix} C_{xx} & 0 & 0 \\ 0 & C_{yy} & C_{yz} \\ 0 & C_{yz} & C_{zz} \end{bmatrix} . \tag{26}$$

A big advantage of expressing the interactions in terms of local axes is that all single-ion anisotropies and all nn interaction matrices are identical (apart from transposing if site indices are interchanged). Using the three-fold axis and inversion symmetry we find that

$$\begin{aligned} \mathcal{I}_{1,2} \ &= \ \mathcal{I}_{2,3} = \mathcal{I}_{3,1} = \tilde{\mathcal{I}}_{2,1} = \tilde{\mathcal{I}}_{3,2} = \tilde{\mathcal{I}}_{1,3} \\ &= \ \mathcal{I}_{4,3} = \mathcal{I}_{5,4} = \mathcal{I}_{3,5} = \tilde{\mathcal{I}}_{3,4} = \tilde{\mathcal{I}}_{4,5} = \tilde{\mathcal{I}}_{5,3} . \end{aligned} \tag{27}$$

where the sites are numbered as in Fig. 10.

Just as for nearest neighbors, all the next nearest neighbor interaction matrices are the same, providing we take the indices in the correct order.

C. Canting

Up to now we have taken the local z-axes to lie in the Kagomé plane. However, the matrix elements $E_{yz}^{(n)}$ for $n = 1$ or $n = 2$ gives rise to a field which induces a uniform y component of spin. For the spin-wave calculation it is convenient to define "canted local axes" such that the canted z-axes lie along the direction of the canted spins. This direction is found by minimizing the

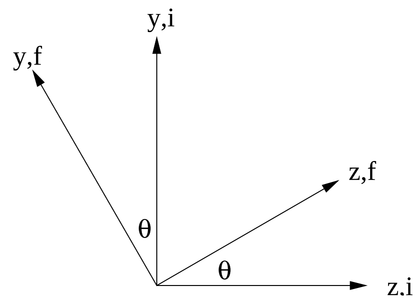

FIG. 11: The 'initial' and 'final' local y and z axes. Initially the z axis is in the Kagomé plane. The sign of θ is the same that of H_y, which is the negative of $E_{yz}^{(1)}$, i .e. the negative of D_y.

energy. We write the ground state energy per site, E_G, for $S_z = S\cos\theta$ and $S_y = S\sin\theta$ as

$$\begin{aligned} E_G/S^2 &= [C_{zz} - 2E_z^{(1)} - 2E_z^{(2)}]\cos^2\theta \\ &\quad +[C_{yy} - 2E_y^{(1)} - 2E_y^{(2)}]\sin^2\theta \\ &\quad +2[C_{yz} + 2E_{yz}^{(1)} + 2E_{yz}^{(2)}]\sin\theta\cos\theta \\ &\equiv -A_{cc}\cos^2\theta - A_{ss}\sin^2\theta + 2A_{cs}\sin\theta\cos\theta \\ &= -\frac{1}{2}[A_{cc} + A_{ss}] - H_z\cos(2\theta) \\ &\quad -H_y\sin(2\theta) , \end{aligned} \tag{28}$$

where

$$H_z = [A_{cc} - A_{ss}]/2 , \quad H_y = -A_{cs} . \tag{29}$$

The energy is minimized by setting

$$\cos(2\theta) = H_z/H , \quad \sin(2\theta) = H_y/H , \tag{30}$$

where $H = \sqrt{H_z^2 + H_y^2}$. If we neglect the effect of anisotropic nnn interactions on the canting angle, we have

$$\begin{aligned} H_y &= -[C_{yz} + 2E_{yz}^{(1)}] = -C_{yz} - \sqrt{3}D_y + J_{yz} \\ H_z &= E_z^{(1)} - E_y^{(1)} - \frac{1}{2}C_{zz} + \frac{1}{2}C_{yy} \\ &\quad +E_z^{(2)} - E_y^{(2)} \\ &= \frac{3}{2}J_1 - \frac{\sqrt{3}}{2}D_z + \frac{C_{y-z}}{2} + \frac{3}{2}J_2 + \frac{3\Delta_J - \eta_J}{8} \end{aligned} \tag{31}$$

where $C_{\alpha-\beta} \equiv C_{\alpha\alpha} - C_{\beta\beta}$. Here and below the superscript "1" for nn's is implied in the anisotropic interactions.

This means that we want to transform the initial local coordinates with moments in the Kagomé plane into the canted local coordinates via

$$\begin{aligned} S_z^{\rm loc,i} &= cS_z^{\rm loc,f} - sS_y^{\rm loc,f} \\ S_y^{\rm loc,i} &= sS_z^{\rm loc,f} + cS_y^{\rm loc,f} , \end{aligned} \tag{32}$$

as illustrated in Fig. 11, where $c \equiv \cos\theta$ and $s \equiv \sin\theta$. Then, if we include this transformation we finally arrive at the local anisotropy matrix as

$$\overline{\mathbf{C}} = \begin{bmatrix} C_{xx} & 0 & 0 \\ 0 & \overline{C}_{yy} & \overline{C}_{yz} \\ 0 & \overline{C}_{yz} & \overline{C}_{zz} \end{bmatrix} , \tag{33}$$

and the transformed local interaction matrices are

$$\overline{\mathcal{I}}_{1,2} = \begin{bmatrix} -E_x^{(1)} & \overline{d}_z^{(1)} & -\overline{d}_y^{(1)} \\ -\overline{d}_z^{(1)} & -\overline{E}_y^{(1)} & \overline{E}_{yz}^{(1)} \\ \overline{d}_y^{(1)} & \overline{E}_{yz}^{(1)} & -\overline{E}_z^{(1)} \end{bmatrix} , \tag{34}$$

and similarly for $\overline{\mathcal{I}}_{5,2}$, where

$$\begin{aligned} \overline{C}_{zz} &= c^2C_{zz} + s^2C_{yy} + 2csC_{yz} , \\ \overline{E}_z^{(n)} &= c^2E_z^{(n)} + s^2E_y^{(n)} - 2csE_{yz}^{(n)} , \\ \overline{C}_{yy} &= s^2C_{zz} + c^2C_{yy} - 2csC_{yz} , \\ \overline{E}_y^{(n)} &= s^2E_z^{(n)} + c^2E_y^{(n)} + 2csE_{yz}^{(n)} , \\ \overline{C}_{yz} &= C_{yz}\cos(2\theta) + \frac{1}{2}[C_{yy} - C_{zz}]\sin(2\theta) , \\ \overline{E}_{yz}^{(n)} &= E_{yz}^{(n)}\cos(2\theta) + \frac{1}{2}[E_z^{(n)} - E_y^{(n)}]\sin(2\theta) \\ \overline{d}_z^{(n)} &= cd_z^{(n)} + sd_y^{(n)} \\ \overline{d}_y^{(n)} &= cd_y^{(n)} - sd_z^{(n)} . \end{aligned} \tag{35}$$

An equivalent condition for equilibrium is that

$$\overline{C}_{yz} + 2\sum_n \overline{E}_{yz}^{(n)} = 0 . \tag{36}$$

When the x-z elements are summed over all neighbors they give a vanishing effective field. Indeed, group theory guarantees that this is the case for general interactions.

IV. CALCULATION OF THE SPIN WAVE SPECTRUM

In Appendix A we write the Hamiltonian in terms of boson operators and in Appendix B we obtain the wavevector dependent spin-wave dynamical matrix (SWDM) $\mathbf{M}(\mathbf{q})$ whose eigenvalues are the spin-wave energies at wavevector $\mathbf{q}$ and which is written as

$$\mathbf{M}(\mathbf{q}) = \left[\begin{array}{c|c} \mathbf{A}(\mathbf{q}) & -\mathbf{B}(\mathbf{q}) \\ \hline \mathbf{B}(\mathbf{q})^* & -\mathbf{A}(\mathbf{q})^* \end{array}\right] . \tag{37}$$

A. General Form of the Spin-Wave Dynamical Matrix

The matrices $\mathbf{A}(\mathbf{q})$ and $\mathbf{B}(\mathbf{q})$ are given in Eqs. (A7) and (A8), respectively. We write them as

$$\mathbf{A}(\mathbf{q}) = \overline{\Delta}\mathcal{E} + \sum_n \mathbf{A}^{(n)}(\mathbf{q}) \tag{38}$$

and

$$\mathbf{B}(\mathbf{q}) \;=\; (C_{xx} - \overline{C}_{yy})\mathcal{E} + \sum_n \mathbf{B}^{(n)}(\mathbf{q}) \;, \tag{39}$$

where $\overline{\Delta} = C_{xx} + \overline{C}_{yy} - 2\overline{C}_{zz}$, $\mathcal{E}$ is the unit matrix, and for $n = 1$ or 2 $\mathbf{A}^{(n)}(\mathbf{q})$ is

$$\left[\begin{array}{c|c|c} 4\overline{E}_z^{(n)} & [-E_x^{(n)} - \overline{E}_y^{(n)} & [-E_x^{(n)} - \overline{E}_y^{(n)} \\ & -2i\overline{d}_z^{(n)}]\gamma_{1,2}^{(n)}(\mathbf{q}) & +2i\overline{d}_z^{(n)}]\gamma_{1,3}^{(n)}(\mathbf{q}) \\ \hline [-E_x^{(n)} - \overline{E}_y^{(n)} & 4\overline{E}_z^{(n)} & [-E_x^{(n)} - \overline{E}_y^{(n)} \\ +2i\overline{d}_z^{(n)}]\gamma_{1,2}^{(n)}(\mathbf{q}) & & -2i\overline{d}_z^{(n)}]\gamma_{2,3}^{(n)}(\mathbf{q}) \\ \hline [-E_x^{(n)} - \overline{E}_y^{(n)} & [-E_x^{(n)} - \overline{E}_y^{(n)} & 4\overline{E}_z^{(n)} \\ -2i\overline{d}_z^{(n)}]\gamma_{1,3}^{(n)}(\mathbf{q}) & +2i\overline{d}_z^{(n)}]\gamma_{2,3}^{(n)}(\mathbf{q}) & \end{array}\right] , \tag{40}$$

and $\mathbf{B}^{(n)}(\mathbf{q})$ is

$$\left[\begin{array}{c|c|c} 0 & [-E_x^{(n)} + \overline{E}_y^{(n)}] & [-E_x^{(n)} + \overline{E}_y^{(n)}] \\ & \times\gamma_{1,2}^{(n)}(\mathbf{q}) & \times\gamma_{1,3}^{(n)}(\mathbf{q}) \\ \hline [-E_x^{(n)} + \overline{E}_y^{(n)}] & 0 & [-E_x^{(n)} + \overline{E}_y^{(n)}] \\ \times\gamma_{1,2}^{(n)}(\mathbf{q}) & & \times\gamma_{2,3}^{(n)}(\mathbf{q}) \\ \hline [-E_x^{(n)} + \overline{E}_y^{(n)}] & [-E_x^{(n)} + \overline{E}_y^{(n)}] & 0 \\ \times\gamma_{1,3}^{(n)}(\mathbf{q}) & \times\gamma_{2,3}^{(n)}(\mathbf{q}) & \end{array}\right] , \tag{41}$$

where $\gamma_{\tau,\tau'}^{(n)}(\mathbf{q})$ is the normalized form factor for the nth shell of neighbors. Here we we will only treat $n = 1, 2$. For in-plane interactions we have

$$\begin{aligned} \gamma_{12}^{(1)}(\mathbf{q}) &= \cos(aq_x/2) \;, \\ \gamma_{13}^{(1)}(\mathbf{q}) &= \cos[a(q_x + \sqrt{3}q_y)/4] \;, \\ \gamma_{23}^{(1)}(\mathbf{q}) &= \cos[a(q_x - \sqrt{3}q_y)/4] \;, \\ \gamma_{12}^{(2)}(\mathbf{q}) &= \cos(aq_y\sqrt{3}/2) \;, \\ \gamma_{13}^{(2)}(\mathbf{q}) &= \cos[a(3q_x - \sqrt{3}q_y)/4] \;, \\ \gamma_{23}^{(2)}(\mathbf{q}) &= \cos[a(3q_x + \sqrt{3}q_y)/4] \;. \end{aligned} \tag{42}$$

In Eqs. (40) and (41) one one uses Eq. (35) to relate the overlined coefficients to the bare coefficients, which are defined in Eqs. (33) and (24).

To simplify the expressions we will now specialize to the case when the nnn interactions are isotropic and all interactions further than nnn are ignored. Then we write the matrix $\mathbf{A}(\mathbf{q})$ in the form

$$\left[\begin{array}{c|c|c} A_0 + 2J_2 & (A_1 - i\alpha_1)\gamma_{12}^{(1)} + & (A_1 + i\alpha_1)\gamma_{13}^{(1)} + \\ & \left(\frac{1}{2}J_2 - i\alpha_2\right)\gamma_{12}^{(2)} & \left(\frac{1}{2}J_2 - i\alpha_2\right)\gamma_{13}^{(2)} \\ \hline (A_1 + i\alpha_1)\gamma_{12}^{(1)} + & A_0 + 2J_2 & (A_1 - i\alpha_1)\gamma_{23}^{(1)} + \\ \left(\frac{1}{2}J_2 + i\alpha_2\right)\gamma_{12}^{(2)} & & \left(\frac{1}{2}J_2 - i\alpha_2\right)\gamma_{23}^{(2)} \\ \hline (A_1 - i\alpha_1)\gamma_{13}^{(1)} + & (A_1 + i\alpha_1)\gamma_{23}^{(1)} + & A_0 + 2J_2 \\ \left(\frac{1}{2}J_2 - i\alpha_2\right)\gamma_{13}^{(2)} & \left(\frac{1}{2}J_2 + i\alpha_2\right)\gamma_{23}^{(2)} & \end{array}\right] , \tag{43}$$

where $\gamma_{nm}^{(k)}$ denotes $\gamma_{nm}^{(k)}(\mathbf{q})$. The matrix $\mathbf{B}(\mathbf{q})$ is of the form

$$\left[\begin{array}{c|c|c} B_0 & B_1\gamma_{12}^{(1)}(\mathbf{q}) & B_1\gamma_{13}^{(1)}(\mathbf{q}) \\ & -\frac{3}{2}J_2\gamma_{12}^{(2)}(\mathbf{q}) & -\frac{3}{2}J_2\gamma_{13}^{(2)}(\mathbf{q}) \\ \hline B_1\gamma_{12}^{(1)}(\mathbf{q}) & B_0 & B_1\gamma_{23}^{(1)}(\mathbf{q}) \\ -\frac{3}{2}J_2\gamma_{12}^{(2)}(\mathbf{q}) & & -\frac{3}{2}J_2\gamma_{23}^{(2)}(\mathbf{q}) \\ \hline B_1\gamma_{13}^{(1)}(\mathbf{q}) & B_1\gamma_{23}^{(1)}(\mathbf{q}) & B_0 \\ -\frac{3}{2}J_2\gamma_{13}^{(2)}(\mathbf{q}) & -\frac{3}{2}J_2\gamma_{23}^{(2)}(\mathbf{q}) & \end{array}\right] . \tag{44}$$

In Appendix C we evaluate of the constants in the matrices for the general Hamiltonian introduced above. In the interest of simplicity we now limit consideration to the following generic Hamiltonian:

$$\begin{aligned} \mathcal{H} \;=\; & \sum_{i<j\in nn} \Big[J_1 S_i \cdot S_j + D_{ij} \cdot S_i \times S_j \Big] \\ & + \sum_{k<l\in nnn} J_2 S_k \cdot S_l \\ & + \; D\sum_i (S_i^{y'})^2 - E\sum_i [(S_i^{z'})^2 - (S_i^{x'})^2] \end{aligned} \tag{45}$$

where $\in$ nn ($\in$ nnn) indicates that the sum is over nn's (nnn's), $D_{ij} = (0, D_y(i,j), D_z(i,j))$ is the Dzyaloskinskii-Moriya vector for bond $i-j$ as shown in Fig. 9 and the single-ion anisotropy terms are those used by Nishiyama *et al.*[16] in their treatment of the spin-wave spectrum in jarosites. Here the prime-spin components refer to the local axis associated with the rotated oxygen octahedra shown in Fig. 1 (see Ref. 16 for details). The $D_y(i,j)$ and $D_z(i,j)$ are all expressible in terms of the parameters D_y and D_z as discussed in Sec. III. The single-ion anisotropy constants D and E used in Ref. 16 are related to our generic single-ion matrix C defined in the uncanted-local frame given in Eq. (26) as

$$\begin{aligned} C_{xx} &= E \\ C_{xy} &= C_{xz} = C_{yx} = C_{zx} = 0 \\ C_{yy} &= D\cos(\theta_0)^2 - E\sin(\theta_0)^2 \\ C_{yz} &= C_{zy} = (D+E)\sin(\theta_0)\cos(\theta_0) \\ C_{zz} &= D\sin(\theta_0)^2 - E\cos(\theta_0)^2 \;, \end{aligned} \tag{46}$$

where θ_0 is the rotation angle of the octahedra around Fe-ion (see Fig. 2) and is $\theta_0 = 20^{\mathrm{o}}$.[16]

In what follows we will often have recourse to two simple models. In the first of these, which we call the "DM" model, we neglect the single ion anisotropy and the exchange anisotropy, so that the only nonzero parameters are J_1, J_2, D_y, and D_z. In the second model, which we call the "CF" model, all the anisotropy is incorporated by the single-ion crystal field, so that the only nonzero parameters are J_1, J_2, and $C_{\alpha\beta}$. In either case, we assume J_1 to be the dominant interaction. Accordingly we give here the expressions for the matrix elements of the SWDM which pertain to these two cases:

$$A_0 \;=\; 2J_1 + \Delta - 2\sqrt{3}D_z + \frac{2}{3J_1}[3D_y^2 + 2C_{yz}^2] \;,$$

$$
\begin{aligned}
A_1 &= \frac{1}{2}J_1 + \frac{\sqrt{3}}{2}D_z + \frac{1}{6J_1}\left[3D_y^2 - C_{yz}^2\right] , \\
B_0 &= C_{xx} - C_{yy} - \frac{2C_{yz}^2}{3J_1} , \\
B_1 &= -\frac{3}{2}J_1 + \frac{\sqrt{3}}{2}D_z + \frac{C_{yz}^2 - 3D_y^2}{6J_1} , \\
\alpha_1 &= \frac{1}{\sqrt{3}}C_{yz} + \frac{2\sqrt{3}D_yD_z}{3J_1} - \frac{D_yJ_2}{J_1} , \\
\alpha_2 &= \frac{D_yJ_2}{J_1} .
\end{aligned} \tag{47}
$$

where $\Delta = C_{xx} + C_{yy} - 2C_{zz}$.

B. Analytic Results for Zero Wavevector

At zero wavevector the SWDM, $\mathbf{M}$, whose eigenvalues give $(\omega/S) \equiv \tilde{\omega}$, is

$$
\left[\begin{array}{ccc|ccc}
A_0 & A_1 - i\alpha & A_1 + i\alpha & -B_0 & -B_1 & -B_1 \\
A_1 + i\alpha & A_0 & A_1 - i\alpha & -B_1 & -B_0 & -B_1 \\
A_1 - i\alpha & A_1 + i\alpha & A_0 & -B_1 & -B_1 & -B_0 \\
\hline
B_0 & B_1 & B_1 & -A_0 & -A_1 - i\alpha & -A_1 + i\alpha \\
B_1 & B_0 & B_1 & -A_1 + i\alpha & -A_0 & -A_1 - i\alpha \\
B_1 & B_1 & B_0 & -A_1 - i\alpha & -A_1 + i\alpha & -A_0
\end{array}\right] , \tag{48}
$$

where $\alpha = \alpha_1 + \alpha_2$ and we include the effects of J_2 by replacing J_1 in Eq. (47) everywhere by $J_1 + J_2$. Take $|1\rangle$ to have components $(1,1,1,0,0,0)/\sqrt{3}$ and $|2\rangle$ to have components $(0,0,0,1,1,1)/\sqrt{3}$. Then

$$
\begin{aligned}
\mathbf{M}|1\rangle &= (A_0 + 2A_1)|1\rangle + (B_0 + 2B_1)|2\rangle \\
\mathbf{M}|2\rangle &= (-B_0 - 2B_1)|1\rangle + (-A_0 - 2A_1)|2\rangle .
\end{aligned} \tag{49}
$$

From this we find the spin-wave energy $\tilde{\omega}_0$ to be

$$
(\tilde{\omega}_0)^2 = (A_0 + 2A_1)^2 - (B_0 + 2B_1)^2 . \tag{50}
$$

Now take $|3\rangle$ to have components $(2,-1,-1,0,0,0)/\sqrt{6}$, $|4\rangle$ to have components $(0,0,0,2,-1,-1)/\sqrt{6}$, $|5\rangle$ to have components $(0,1,-1,0,0,0)/\sqrt{2}$, and $|6\rangle$ to have components $(0,0,0,0,1,-1)/\sqrt{2}$. In this subspace

$$
\mathbf{M} = \left[\begin{array}{cccc}
a & b & i\sqrt{3}\alpha & 0 \\
-b & -a & 0 & i\sqrt{3}\alpha \\
-i\sqrt{3}\alpha & 0 & a & b \\
0 & -i\sqrt{3}\alpha & -b & -a
\end{array}\right] , \tag{51}
$$

where $a = A_0 - A_1$, $b = B_0 - B_1$, and $\alpha = \alpha_1 + \alpha_2$. Thereby we find that the other two spin-wave energies, $\tilde{\omega}_\pm$, are given by

$$
\tilde{\omega}_\pm = \sqrt{a^2 - b^2} \pm \sqrt{3}\alpha . \tag{52}
$$

Thus for zero wavevector we find the frequencies $\tilde{\omega}$ for the DM and CF models to be those given in Table I (under the heading "With Canting").

When α is nonzero, we split the degeneracy between the two heretofore degenerate frequencies. This splitting is linear in α. In contrast, when $\alpha = 0$, the splitting between this two-fold degenerate mode and the other mode will be found to be of order $\sqrt{J_1\delta}$, where δ involves anisotropic exchange or DM interactions.

Note that for $\mathbf{C} = 0$, we have stability for $D_z < D_{zc}$, where

$$
\frac{D_{zc}}{J} = \frac{\sqrt{3}}{6}\left(\frac{D_y}{J}\right)^2 + \mathcal{O}[(D_y/J)^4] , \tag{53}
$$

which is similar to Elhajal et al[20] who give $D_{zc}/J \approx 0.22(D_z/J)^2$. For $\mathbf{D} = 0$, we have stability (in the large J limit) if both $C_{xx} - C_{zz}$ and $C_{yy} - C_{zz}$ are positive, so that the z-axis is really the easiest axis.

C. Results for Other Wavevectors

1. The X Point

The X point is at

$$
q_x = [4\pi/(3a)] , \quad q_y = q_z = 0 \tag{54}
$$

and the form factors are

$$
\gamma_{1,2}^{(1)} = -\frac{1}{2} , \quad \gamma_{2,3}^{(1)} = \frac{1}{2} , \quad \gamma_{1,3}^{(1)} = \frac{1}{2} , \tag{55}
$$

and

$$
\gamma_{1,2}^{(2)} = 1 , \quad \gamma_{2,3}^{(2)} = -1 , \quad \gamma_{1,3}^{(2)} = -1 . \tag{56}
$$

Thus the SWDM is of the form

$$
\left[\begin{array}{|c|c|c|c|c|c|}
\hline
a_{11} & a_{12} & -a_{12}^* & -b_{11} & -b_{12} & b_{12} \\
\hline
a_{12}^* & a_{11} & -a_{12} & -b_{12} & -b_{11} & b_{12} \\
\hline
-a_{12} & -a_{12}^* & a_{11} & b_{12} & b_{12} & -b_{11} \\
\hline
b_{11} & b_{12} & -b_{12} & -a_{11} & -a_{12}^* & a_{12} \\
\hline
b_{12} & b_{11} & -b_{12} & -a_{12} & -a_{11} & a_{12}^* \\
\hline
-b_{12} & -b_{12} & b_{11} & a_{12}^* & a_{12} & -a_{11} \\
\hline
\end{array}\right] , \tag{57}
$$

where, to the same accuracy as before

$$
\begin{aligned}
a_{11} &= A_0 + 2J_2 , \\
&= 2(J_1 + J_2) - 2\sqrt{3}D_z + \Delta \\
&\quad +2D_y^2/J_1 + 4C_{yz}^2/(3J_1) ,
\end{aligned} \tag{58}
$$

$$
\begin{aligned}
a_{12} &= -[A_1 - i\alpha_1]/2 + J_2/2 - i\alpha_2 , \\
&= -\frac{1}{4}J_1 + \frac{1}{2}J_2 - \frac{\sqrt{3}}{4}D_z - \frac{D_y^2}{4J_1} \\
&\quad -C_{yz}^2/(12J_1) - \frac{3i}{2}\frac{D_yJ_2}{J_1} \\
&\quad +i\sqrt{3}[C_{yz} + 2(D_yD_z/J_1)]/6 \\
&\equiv a_{12}' + ia_{12}''
\end{aligned} \tag{59}
$$

TABLE I: Spin wave energies $\tilde{\omega} \equiv \omega/S$ for zero wavevector for the DM model (only J_1, J_2, D_y, and D_z nonzero) and for the CF model (only J_1, J_2 and $C_{\alpha\beta}$ nonzero). The results neglecting canting are discussed in subsection IVE. Here $J \equiv J_1 + J_2$. In this and succeeding tables $C_{\alpha-\beta}$ denotes $C_{\alpha\alpha} - C_{\beta\beta}$.

With Canting		
	DM Model	CF Model
$\tilde{\omega}_0$	$\sqrt{12}\lvert D_y\rvert + \mathcal{O}(D^2/J)$	$\left[12JC_{x-z} + 4C_{x-z}C_{y-z} + 4C_{yz}^2\right]^{1/2} + \mathcal{O}(C^{5/2}/J^{3/2})$
$\frac{\tilde{\omega}_+ + \tilde{\omega}_-}{2}$	$\sqrt{-6\sqrt{3}JD_z + 3D_y^2 + 18D_z^2} + \mathcal{O}(D^{5/2}/J^{3/2})$	$\left[6JC_{y-z} + 4C_{x-z}C_{y-z} + 7C_{yz}^2\right]^{1/2} + \mathcal{O}(C^{5/2}/J^{3/2})$
$\tilde{\omega}_+ - \tilde{\omega}_-$	$4D_yD_z/J + \mathcal{O}(D^3/J^2)$	$2C_{yz} + \mathcal{O}(C^2/J)$
Neglecting Canting		
	DM Model	CF Model
$\tilde{\omega}_0$	0	$[12JC_{x-z} + 4C_{x-z}C_{y-z}]^{1/2}$
$\frac{\tilde{\omega}_+ + \tilde{\omega}_-}{2}$	$\sqrt{-6\sqrt{3}JD_z + 18D_z^2}$	$[6JC_{y-z} + 4C_{x-z}C_{y-z}]^{1/2}$
$\tilde{\omega}_+ - \tilde{\omega}_-$	$2\sqrt{3}D_y$	0

TABLE II: Spin wave energies $\tilde{\omega} \equiv \omega/S$ at the X point for the DM and CF models. Here J_2 is considered to be of the same order as D or C. The results neglecting canting are discussed in Sec. IVE.

With Canting		
	DM Model	CF Model
$\tilde{\omega}_0$	$\left[6J_1(3J_2 - \sqrt{3}D_z) + 3D_y^2 - 18\sqrt{3}J_2D_z + 18D_z^2\right]^{1/2} + \mathcal{O}(D^{5/2}/J^{3/2})$	$\left[6J_1(3J_2 + C_{y-z}) + 4C_{x-z}C_{y-z} + 7C_{yz}^2 + 12J_2C_{x-z}\right]^{1/2} + \mathcal{O}(C^{5/2}/J^{3/2})$
$\frac{\tilde{\omega}_+ + \tilde{\omega}_-}{2}$	$\frac{3\sqrt{2}}{2}[J_1 + J_2] - \frac{5\sqrt{6}}{4}D_z + \mathcal{O}(D^2/J)$	$\frac{3\sqrt{2}}{2}[J_1 + J_2] + \frac{\sqrt{2}}{2}(2C_{x-z} + C_{y-z}) + \mathcal{O}(C^2/J)$
$\tilde{\omega}_+ - \tilde{\omega}_-$	$\frac{(2D_yD_z - 3\sqrt{3}D_yJ_2)}{J_1} + \mathcal{O}(D^3/J^2)$	$C_{yz} + \mathcal{O}(C^2/J)$
Neglecting Canting		
	DM Model	CF Model
$\tilde{\omega}_0$	$\left[6J_1(3J_2 - \sqrt{3}D_z) - 18\sqrt{3}J_2D_z + 18D_z^2\right]^{1/2}$	$[6J_1(3J_2 + C_{y-z}) + 4C_{x-z}C_{y-z} + 12J_2C_{x-z}]^{1/2}$
$\frac{\tilde{\omega}_+ + \tilde{\omega}_-}{2}$	$\frac{3\sqrt{2}}{2}[J_1 + J_2] - \frac{5\sqrt{6}}{4}D_z + \mathcal{O}(D^2/J)$	$\frac{3\sqrt{2}}{2}[J_1 + J_2] + \frac{\sqrt{2}}{2}(2C_{x-z} + C_{y-z}) + \mathcal{O}(C^2/J)$
$\tilde{\omega}_+ - \tilde{\omega}_-$	$\sqrt{3}D_y$	0

$$b_{11} = B_0 = C_{xx} - C_{yy} - 2C_{yz}^2/(3J_1) \ , \qquad (60)$$

and

$$\begin{aligned} b_{12} &= -B_1/2 - (3/2)J_2 \ , \\ &= \frac{3}{4}J_1 - \frac{3}{2}J_2 - \frac{\sqrt{3}}{4}D_z + \frac{D_y^2}{4J_1} \\ &\quad + C_{yz}^2/(12J_1) \ , \end{aligned} \qquad (61)$$

where we have neglected symmetric anisotropic exchange and only kept terms that seem to be most relevant.

Now we diagonalize the submatrices $\mathbf{a}$, $\mathbf{a}^*$, and $\mathbf{b}$. The eigenvectors of these 3×3 matrices are

$$\phi_\lambda = \frac{1}{\sqrt{3}} \begin{bmatrix} \lambda \\ 1 \\ -\lambda^2 \end{bmatrix} \ , \qquad (62)$$

where $\lambda^3 = 1$, so that $\lambda_1 = 1$, $\lambda_2 = (-1 + i\sqrt{3})/2$, and $\lambda_3 = (-1 - i\sqrt{3})/2$. One can show that the vector given in Eq. (62) is an eigenvector of $\mathbf{a}$ with the associated eigenvalue

$$a(\lambda) = a_{11} + \lambda^2 a_{12} + \lambda a_{12}^* \ . \qquad (63)$$

and is simultaneously an eigenvector of $\mathbf{b}$ with eigenvalue

$$b(\lambda) = b_{11} + \lambda^2 b_{12} + \lambda b_{12} \ . \qquad (64)$$

The three spin-wave energies are given by

$$\begin{aligned} \tilde{\omega}^2 &= \left[\left(\frac{a(\lambda) + a(\lambda^*)}{2}\right)^2 - b(\lambda)^2\right]^{1/2} \\ &\quad + \left(\frac{a(\lambda) - a(\lambda^*)}{2}\right) \ . \end{aligned} \qquad (65)$$

so that

$$\begin{aligned} \tilde{\omega}_0 &= [(a_{11} + 2a'_{12})^2 - (b_{11} + 2b_{12})^2]^{1/2} \ , \\ \tilde{\omega}_\pm &= [(a_{11} - a'_{12})^2 - (b_{11} - b_{12})^2]^{1/2} \pm \sqrt{3}a''_{12} \ . \end{aligned} \qquad (66)$$

We thus find the spin-wave energies to be those given in Table II.

2. The Y Point

The Y point is at $q_y = 2\pi/(\sqrt{3}a)$, $q_x = q_z = 0$, so that $\gamma_{1,3}^{(n)} = 0$, $\gamma_{2,3}^{(n)} = 0$, $\gamma_{1,2}^{(1)} = 1$, and $\gamma_{1,2}^{(2)} = -1$. Therefore the SWDM at the Y point is of the form

$$\begin{array}{|c|c|c|c|c|c|} a_{11} & a_{12} & 0 & -b_{11} & -b_{12} & 0 \\ \hline a_{12}^* & a_{11} & 0 & -b_{12} & -b_{11} & 0 \\ \hline 0 & 0 & a_{11} & 0 & 0 & -b_{11} \\ \hline b_{11} & b_{12} & 0 & -a_{11} & -a_{12}^* & 0 \\ \hline b_{12} & b_{11} & 0 & -a_{12} & -a_{11} & 0 \\ \hline 0 & 0 & b_{11} & 0 & 0 & -a_{11} \end{array} \ , \tag{67}$$

where

$$\begin{aligned} a_{11} &= A_0 + 2J_2 \ , \\ &= 2(J_1+J_2) - 2\sqrt{3}D_z + \Delta \\ &\quad +2D_y^2/J_1 + 4C_{yz}^2/(3J_1) \ , \end{aligned} \tag{68}$$

$$\begin{aligned} a_{12} &= [A_1 - i\alpha_1] - J_2/2 + i\alpha_2 \ , \\ &= (J_1 - J_2)/2 + \frac{\sqrt{3}}{2}D_z + \frac{D_y^2}{2J_1} - \frac{C_{yz}^2}{6J_1} \\ &\quad -i\sqrt{3}[C_{yz} + 2(D_yD_z/J_1) - 2D_yJ_2/J_1]/3 \\ &\equiv a_{12}' + ia_{12}'' \end{aligned} \tag{69}$$

$$b_{11} = B_0 = C_{xx} - C_{yy} - 2C_{yz}^2/(3J_1) \ , \tag{70}$$

and

$$\begin{aligned} b_{12} &= B_1 + \frac{3}{2}J_2 \\ &= \frac{3}{2}(J_2 - J_1) + \frac{\sqrt{3}}{2}D_z + \frac{C_{yz}^2 - 3D_y^2}{6J_1} \ . \end{aligned} \tag{71}$$

One root for $(\tilde{\omega})^2$ (coming from rows and columns #3 and #6) is

$$\tilde{\omega}_0^2 = a_{11}^2 - b_{11}^2 \tag{72}$$

and the remaining eigenvalues come from the projection of the SWDM, $\mathbf{M}$, into the remaining subspace:

$$\mathbf{M} = \left[\begin{array}{c|c|c|c} a_{11} & a_{12} & -b_{11} & -b_{12} \\ \hline a_{12}^* & a_{11} & -b_{12} & -b_{11} \\ \hline b_{11} & b_{12} & -a_{11} & -a_{12}^* \\ \hline b_{12} & b_{11} & -a_{12} & -a_{11} \end{array}\right] \ . \tag{73}$$

As usual, in our analytic work, we work to second order in the anisotropies, in the absence of which $a_{12} = a_{12}' + ia_{12}''$ is real. In that case we have the unperturbed mode energies

$$(\tilde{\omega}_\pm^{(0)})^2 = (a_{11} \pm a_{12}')^2 - (b_{11} \pm b_{12})^2 \ . \tag{74}$$

The perturbed (i. e. for $a_{12}'' \neq 0$) secular equation is

$$\begin{aligned} 0 &= [\tilde{\omega}^2 - (\tilde{\omega}_-^{(0)})^2][\tilde{\omega}^2 - (\tilde{\omega}_+^{(0)})^2] + (a_{12}'')^4 \\ &\quad -2(a_{12}'')^2[\tilde{\omega}^2 + a_{11}^2 - (a_{12}')^2 - b_{11}^2 + b_{12}^2] \ . \end{aligned} \tag{75}$$

Thereby we find the approximate solutions

$$\begin{aligned} \tilde{\omega}_\pm &= \tilde{\omega}_\pm^{(0)} \pm \frac{(a_{12}'')^2}{\tilde{\omega}_\pm^{(0)}[(\tilde{\omega}_+^{(0)})^2 - (\tilde{\omega}_-^{(0)})^2]} \\ &\quad \times \left[(\tilde{\omega}_\pm^{(0)})^2 + a_{11}^2 - (a_{12}')^2 - b_{11}^2 + b_{12}^2\right] \ . \end{aligned} \tag{76}$$

In Table III we give analytical results correct only to leading order in the anisotropies, in which case $\tilde{\omega}_\pm = \tilde{\omega}_\pm^{(0)}$.

V. FIT TO THE EXPERIMENTAL SPECTRUM

Recently Matan *et al.*[22] have measured spin-wave spectrum in FeJ using inelastic neutron scattering and here we discuss the comparison of our calculations with their results. The experimental spectrum[22] shown in Fig. 12 clearly indicates three spin-bands. One of these bands is quite dispersionless and it is therefore identified to be the "zero-energy" mode, which is lifted to about 8 meV due to anisotropic magnetic interactions which we wish to identify. In addition to this "lifted zero-energy mode", the spectrum shows two additional gaps at 1.7 meV (an in-plane mode) and around 7 meV (an out-of-plane mode). The spin-wave spectrum extends up to 20 meV at the X-point. It is of interest to develop a model Hamiltonian which reproduces the observed spectrum. In particular, we will see that the observed energy splittings at the various high symmetry points provide sensitive constraints on the interaction parameters.

In order to identify magnetic interactions in FeJ, in this section, we will present numerical calculations of the spin-wave spectrum for a large number of models and compare the results with the experimental data shown in Fig. 12. For a quantitative comparison we define an error-factor R (i.e. the goodness-of-fit) as follows:

$$R = \frac{100}{N_{\rm data}} \sum_i |\omega_{\rm exp}(q_i) - \omega_{\rm cal}(q_i)|/\omega_{\rm exp}(q_i) \tag{77}$$

where $N_{\rm data}$ is the number of experimental data points, and $\omega_{\rm exp}(q_i)$ and $\omega_{\rm cal}(q_i)$ are respectively the experimental and calculated spin wave energies at wave-vector q_i. One should recognize that R describes the percentage error averaged over the entire spectrum. It is important to reproduce the splittings at the high symmetry points even though this only weakly affects the value of R.

We start by comparing the experimental spectrum to a simple model where we consider only the isotropic nearest neighbor interaction J_1 and a non-zero D_z in DM interaction vector (i.e. $D_x = D_y = 0$). The best fit from this simple two-parameter model is shown in Fig. 13. The DM

TABLE III: Spin wave energies $\tilde{\omega} \equiv \omega/S$ at the Y point for the DM and CF models. The results neglecting canting are discussed in Sec. IVE.

With Canting		
	DM Model	CF Model
$\tilde{\omega}_-$	$\left[12J_1J_2 - 6\sqrt{3}J_1D_z + 4J_2^2 - 14\sqrt{3}J_2D_z + 18D_z^2 + 3D_y^2\right]^{1/2} + \mathcal{O}(D^{5/2}/J^{3/2})$	$\left[12J_1J_2 + 6J_1C_{y-z} + 4C_{x-z}C_{y-z} + 8J_2C_{x-z} + 2J_2C_{y-z} + 4J_2^2 + 7C_{yz}^2\right]^{1/2} + \mathcal{O}(C^{5/2}/J^{3/2})$
$\frac{\tilde{\omega}_+ + \tilde{\omega}_0}{2}$	$2J_1 + \frac{5}{2}J_2 - \frac{7\sqrt{3}}{4}D_z + \mathcal{O}(D^2/J)$	$2J_1 + \frac{5}{2}J_2 + \frac{1}{4}(6C_{x-z} + 3C_{y-z}) + \mathcal{O}(C^2/J)$
$\tilde{\omega}_+ - \tilde{\omega}_0$	$J_2 + \frac{\sqrt{3}}{2}D_z + \mathcal{O}(D^2/J)$	$J_2 + C_{x-z} - \frac{1}{2}C_{y-z} + \mathcal{O}(C^2/J)$

Neglecting Canting		
	DM Model	CF Model
$\tilde{\omega}_-$	$\left[12J_1J_2 - 6\sqrt{3}J_1D_z + 4J_2^2 - 14\sqrt{3}J_2D_z + 18D_z^2\right]^{1/2}$	$\left[12J_1J_2 + 6J_1C_{y-z} + 4C_{x-z}C_{y-z} + 8J_2C_{x-z} + 2J_2C_{y-z} + 4J_2^2\right]^{1/2}$
$\frac{\tilde{\omega}_+ + \tilde{\omega}_0}{2}$	$2J_1 + \frac{5}{2}J_2 - \frac{7\sqrt{3}}{4}D_z + \mathcal{O}(D^2/J)$	$2J_1 + \frac{5}{2}J_2 + \frac{1}{4}(6C_{x-z} + 3C_{y-z}) + \mathcal{O}(C^2/J)$
$\tilde{\omega}_+ - \tilde{\omega}_0$	$J_2 + \frac{\sqrt{3}}{2}D_z + \mathcal{O}(D^2/J)$	$J_2 + C_{x-z} - \frac{1}{2}C_{y-z} + \mathcal{O}(C^2/J)$

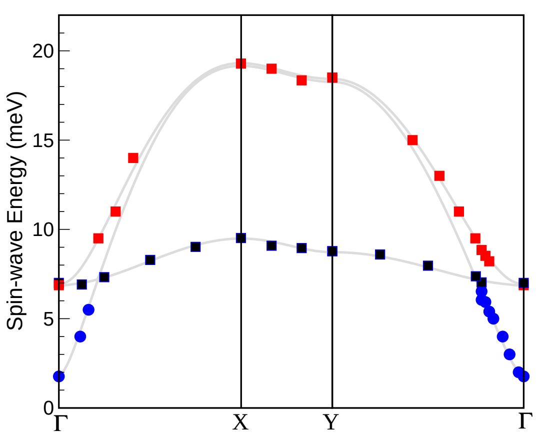

FIG. 12: (Color online) Experimental spin-wave spectrum in FeJ obtained from inelastic neutron scattering measurements.[22] The gray-lines represent the best fit which is discussed in the text in detail.

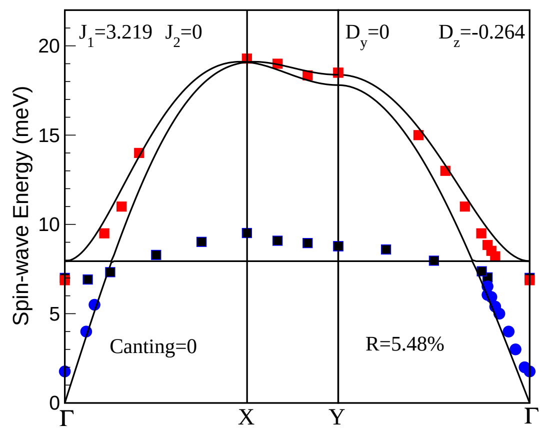

FIG. 13: (Color online) Spin-wave spectrum from a simple two-parameter $J - D_z$ model. In these and succeeding figures the values of the parameters of the fit are given in meV.

interaction with only the D_z term lifts the zero-energy mode to the dispersionless energy $S\sqrt{-6\sqrt{3}JD_z}$, as observed experimentally. However this term alone can not give the experimentally observed small dispersion of this mode. Without D_y, we do not get any canting of spins either. The effect of the D_z term is almost identical to an easy plane anisotropy. The "lifted zero-energy mode" is found to be degenerate with the other spin gap (*i.e.* the out-of-plane spin-gap) at the Γ point. However, we do not get the in-plane gap as experimentally observed at 1.7 meV. (Analytic results are given in Table I.)

The agreement between calculations and experiment can be improved significantly by turning on D_y in the DM-vector as shown in Fig. 14. The main effect of D_y term is to create a small in-plane anisotropy and therefore it can be adjusted to give an in-plane gap of 1.7 meV, as experimentally observed. This model gives three gaps at Γ point, for which the analytic results are given in Table I. From these analytic results, one sees that the in-plane gap is proportional to $|D_y|$ and the small splitting between the flat-mode and the out-of-plane gap is equal to $10D_yD_z/J$, which is quite small.

Although the experiment does not give clear results for the splittings of the high-energy modes at the X and Y points, we see from Table II that the splitting, δ, at the X point is expected to be quite small (it is second order in the perturbations). Table III indicates that the splitting of the high frequency modes at the Y point is expected to be larger than at the X point.

The D_y term also causes the spins to be canted with a

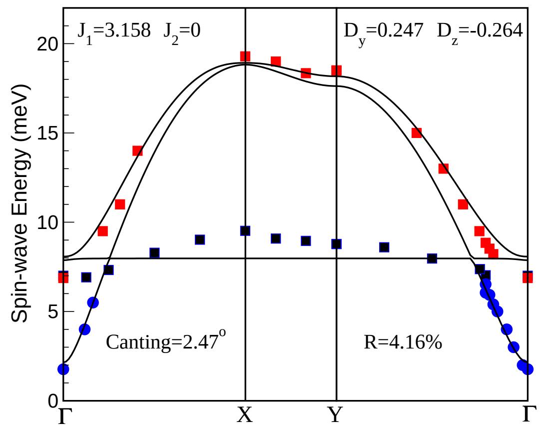

FIG. 14: (Color online) Spin-wave spectrum from a simple three-parameter $J_1 - D_y - D_z$ model.

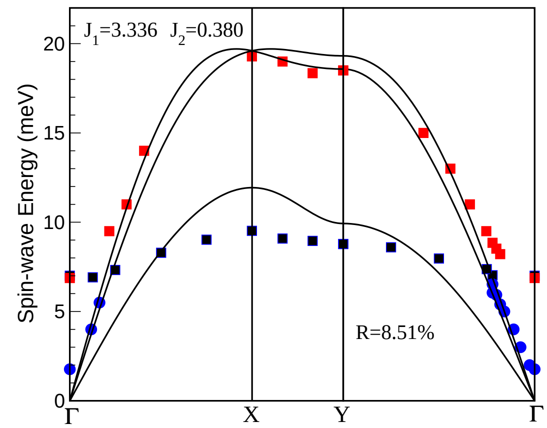

FIG. 15: (Color online) Spin-wave spectrum from isotropic nn and nnn interactions J_1 and J_2.

canting angle of about 2.5°. However despite a significant improvement with the addition of D_y term, we still do not get any dispersion to the flat mode in contradiction to the experimental finding. We also studied the single ion term D and E as given in Eq. (46) with only J_1 and obtained similar results. With only DM or single ion anisotropy without further neighbor interactions, it was not possible to obtain the small dispersion of the flat mode as experimentally observed.

In order to get the experimentally observed dispersion along with the correct average energy of the nearly flat mode, one needs to consider next-nearest neighbor interactions. In Fig. 15, we show the best fit from a simple isotropic nn (J_1) and nnn (J_2) interactions, which is in good agreement with the previous work.[5] We note that the nnn J_2 interaction gives the zero-energy mode a significant dispersion. However in order to correctly reproduce the flat-mode energy requires a J_2 which gives too strong a dispersion. Since the Hamiltonian with isotropic J_1 and J_2 is rotationally invariant, we do not get any gap at the Γ point, in contrast to experimentally observed three gaps.

From above discussion, it is clear that one needs both a nnn J_2 interaction and either a DM or a single ion anisotropy. In Fig. 16, we show the best fit from a model which has the isotropic nn J_1, nnn J_2 interactions and the DM vector $(0, D_y, D_z)$. The fit to the data is very good. We reproduce not only the three gaps but also the small dispersion of the flat-mode. The spin gaps at the Γ, X, and Y points obtained numerically are in good agreement with the analytic results given in Tables I, II, and III. The spin-canting angle is about 2.1°, in reasonable agreement with the experimentally estimated value of 1.5°.[22]

As an alternative to DM interactions, one can also try to explain the experimental data based on a model which considers only the single ion anisotropies D and E as given in Eq. (46).[16] In Fig. 16b, we show the best fit from such a model which has an isotropic nn J_1 and nnn J_2 and the (D, E) single ion anisotropy instead of the DM interactions. The R-factor for this fit is slightly larger than the R-factor obtained from DM interaction. The main differences are the larger splittings of the optical modes at the Γ and X points and the smaller canting angle for the CF model in comparison to the DM model. The canting angle from the CF model is only 0.8°, which is smaller than the experimental value[22] of 1.5°.

The biggest problem with the CF model is the large gaps at the Γ and X-points as shown in Fig. 16b. The experimental splitting of the modes at these points are much smaller. Numerical results give a splitting of about 0.75 meV at the Γ point and 0.4 meV at the X-point. The splitting at the Y-point is quite small. These results are in good agreement with the analytical results given in Tables II and III.

In conclusion, the observed spin-wave spectrum can be explained by a simple model which has only nearest and next-nearest isotropic interactions. The DM interaction gives the best fit to explain the observed gaps and the spin canting. Even though the single ion terms also fit the data well, the quality of the fit is not as good as the one from DM term at the Γ and X points. For the Fe ion, the single ion anisotropy is expected to be smaller than the DM term (because the single-ion term is second order in the spin-orbit coupling while the DM term appears in first order). For these reasons, we think that DM term is a natural source of anisotropy in FeJ compound, which not only stabilizes the observed experimental spin structure but also gives the right spin-wave spectrum with the proper gaps and dispersion.

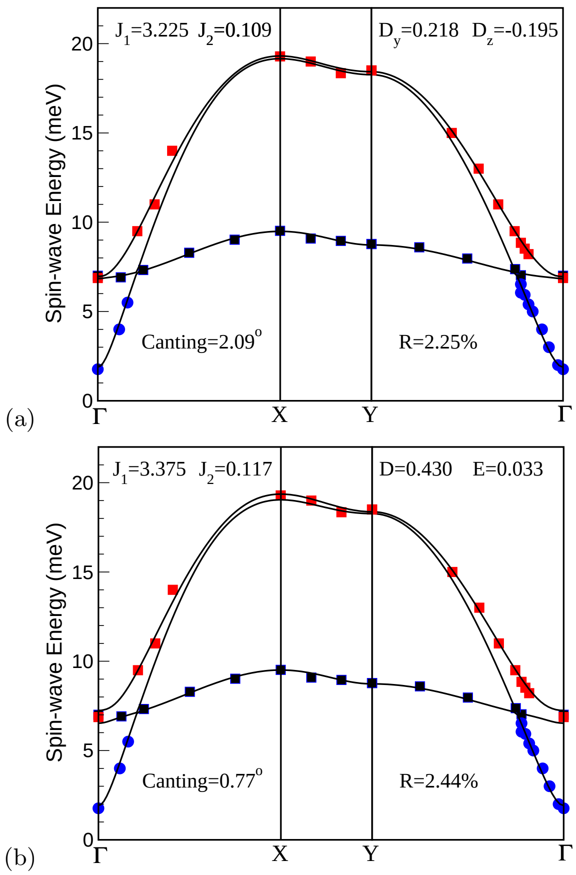

FIG. 16: (Color online) Spin-wave spectrum from isotropic nn and nnn interactions J_1 and J_2 and (a) DM-vector $(0, D_y, D_z)$ and (b) single ion anisotropy terms D and E.

A. Effect of Spin-Canting on the Spin-wave Spectrum

Here we give results when the transformation to the canted structure is omitted, i.e. θ is forced to be zero. One purpose of giving these results is to show the importance of making this transformation when calculating the gaps in the spectrum which depend on small perturbations. Also, we could check our calculations by comparing these results to those of Nishiyama et al[16] who omitted this transformation. When one distorts a collinear spin structure by the application of a small transverse field, the effects on the spectrum are second order in the distortion angle. Here, however, the situation is different because the spins before distortion are noncollinear. As a result of this noncollinearity the matrix element $d_y^{(1)}$ in Eq. (23) (which would be zero for a collinear system) is of order J. Thus the matrix element $\overline{d}_z^{(n)}$ in Eq.(35) has a contribution, $sd_y^{(n)}$, induced by canting of the same order as that, $cd_z^{(n)}$, which existed before canting. This fact indicates that canting should not be ignored in the calculation of the spin-wave spectrum.

To obtain results when canting is ignored we replace quantities with overbars in Eq. (35) by the corresponding quantities without overbars.

1. *Zero wavevector*

Here (where J denotes $J_1 + J_2$)

$$A_0 = 4E_z + \Delta = 2J - 2\sqrt{3}D_z + \Delta \ , \tag{78}$$

$$A_1 = -E_x - E_y = J/2 + \sqrt{3}D_z/2 \ , \tag{79}$$

$$\alpha_1 = 2d_z(1) = -D_y \ , \quad \alpha_2 = 0 \ , \tag{80}$$

$$B_0 = C_{xx} - C_{yy} \ , \tag{81}$$

$$B_1 = E_x - E_y = -3J/2 + \sqrt{3}D_z/2 \ . \tag{82}$$

Then, when the anisotropy in J_n is neglected, we find the frequencies listed in Table I under the heading "Neglecting Canting."

2. *The X point*

The treatment including canting is now modified so that

$$\begin{aligned} a_{11} &= 2(J_1 + J_2) - 2\sqrt{3}D_z + \Delta \ , \\ a_{12} &= -[A_1 - i\alpha_1]/2 + J_2/2 - i\alpha_2 \\ &= -J_1/4 + J_2/2 - \sqrt{3}D_z/4 - iD_y/2 \ , \\ b_{11} &= C_{xx} - C_{yy} \ , \\ b_{12} &= -B_1/2 - 3J_2/2 \\ &= 3J_1/4 - 3J_2/2 - \sqrt{3}D_z/4 \ . \end{aligned} \tag{83}$$

Then we find the spin-wave frequencies as listed in Table II.

3. *The Y point*

Now we have

$$\begin{aligned} a_{11} &= A_{11}(\mathbf{q}=0) = 2(J_1 + J_2) - 2\sqrt{3}D_z + \Delta \ , \\ a_{12} &= A_{12}(\mathbf{q}=0) = (J_1 - J_2)/2 + \sqrt{3}D_z/2 + iD_y \ , \\ b_{11} &= C_{xx} - C_{yy} \ , \\ b_{12} &= -3(J_1 - J_2)/2 + \sqrt{3}D_z/2 \ , \end{aligned} \tag{84}$$

so that the frequencies are those given in Table III. Unless the only anisotropy is due to D_y, these results are the same as those given in Table III with canting, so that, except for this case, the effect of canting at the Y point is very small.

The effect of canting can be deduced from the epxressions for the matrix elemets given in Appendix C. One sees that the rotation to the canted spin structure induces terms of the form D_y^2/J_1 into the SWDM matrix elements. Also the quantity $\alpha_1 \equiv 2\overline{d}_z^{(1)}$ is transformed (by the rotation to the canted system of coordinates) from the value D_y (neglecting the anisotropy in J_n) to $(C_{yz}+2D_zD_y/J_1)\sqrt{3}-D_yJ_2/J_1$. Suprprisingly perhaps, this rotation through an angle of order D_y/J_1 also introduces a contribution to α_2 of order J_2D_y/J_1. A qualitative understanding of what is going on here is obtained by noting that the coefficient $\overline{d}_z$ is associated with an interaction proportional to $S_x^{\rm loc,f}S_y^{\rm loc,f}$, where the components are taken in the "final" *i. e.* canted coordinate system. This term directly affects the spin-wave energies. This term arises from rotating an interaction in the local uncanted coordinate system of the form $d_yS_x^{\rm loc,i}S_z^{\rm loc,i}$, a term which for collinear systems is zero, but for this noncollinear system is of order J_1, as given in Eq. (24). Since these quantities control several of the splittings, it is clear that neglecting canting can have a major impact on these splittings, as shown in Fig. 17 and the tables. From Fig. 16(a), it is clear that the quality of the fit is significantly degraded for the DM term, in particular at the Γ and X-points where big gaps are opened.

The effect of neglecting canting is opposite for the CF term. The quality of the fit is improved because the large splitting at Γ (see Fig. 16(b)) is now zero (Fig. 17(b)). For instance, for zero wavevector the splitting $\tilde{\omega}_+ - \tilde{\omega}_-$ (given by $2\sqrt{3}\alpha$) is linear in D_y when canting is neglected, whereas when the canting was taken into account the splitting was found to be proportional to $C_{yz}+2D_zD_y/J_1$. To calculate this splitting it is therefore not qualitatively correct to ignore the canting. In addition, when canting is ignored and single-ion anisotropy is not present, neglecting canting leads to $\tilde{\omega}_0 = 0$, even when $\mathbf{D}$ is nonzero.

At the X point the effects of canting are similar. For the low energy mode the transformation to the canted structure introduces a term proportional to D_y^2 which is only important if all the other anisotropies are very small or vanishing. However, as Table II indicates, the splitting between $\omega_+ - \omega_-$ is proportional to D_y when canting is neglected, but is proportional to $C_{yz} + 2D_yD_z/J_1 - 3\sqrt{3}J_2D_y/J_1$ when canting is taken into account.

At the Y point the effects of canting are less important. Indeed ω_0 and ω_+ are insensitive to canting and only in ω_- does one see that canting introduces a term of order D_y^2.

In conclusion, it is important that one should not ignore the spin-canting when spin-wave spectrum is calculated. Even though the CF single ion term gives much better fit when the canting is ignored (see Figs. 16 and 17), it is not an appropriate approximation, as we have shown. When the CF single ion term is properly treated, it actually gives a worse fit to the data and therefore it is more logical to conclude that the dominant source of the anisotropy in FeJ compound is the DM term.

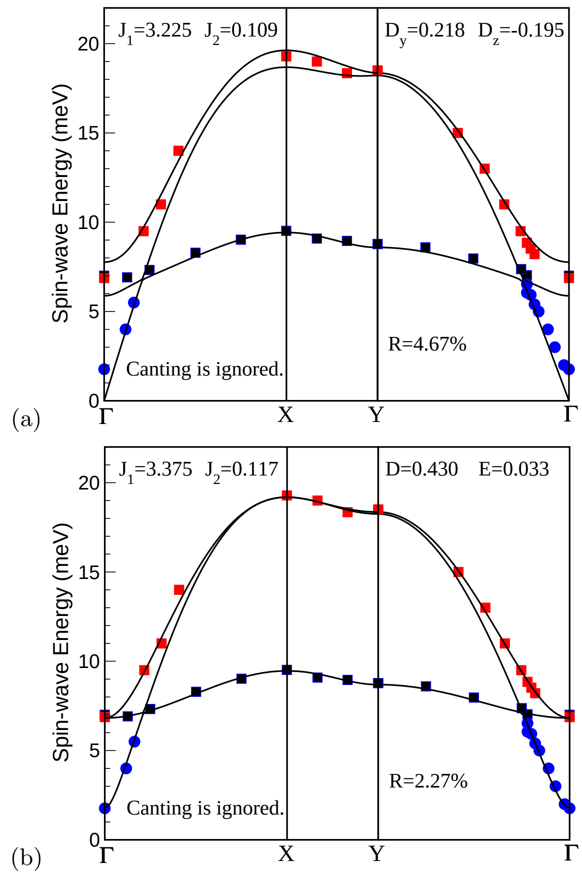

FIG. 17: (Color online) Spin-wave spectrum for the DM (a) and CF (b) models when the spin-canting is ignored. We used the same parameters as in Fig. 16 to emphasize the effect of spin-canting on the spectrum.

VI. CONCLUSIONS

We have presented a detailed study of the magnetic structure and spin-wave spectrum in FeJ for the most generic nn and nnn exchange interactions including Dzyaloshinskii-Moriya and the single ion anisotropy terms of Inami *et al.*[14] Our conclusions can be summarized as follows.

- We first discuss the allowed magnetic structures from a representations analysis. The experimentally observed "umbrella" structure of $\mathbf{q}$=0 with positive chirality arises from a one dimensional representation which exhibits three-fold symmetry. Our analysis and discussion of broken symmetry suggests that the characterization by irreducible representations is more fundamental than that by

chirality, even though chirality has been widely invoked in the literature.

- Representation analysis reveals the existence of an x-y-like two dimensional representation which has sixth order in-plane anisotropy. In this representation one can have Kagomé layers with a net in-plane moment which can be stacked either ferromagnetically or antiferromagnetically. The analysis of Ref. 15 did not find wavefunctions of this type. However, the observed magnetic ground state of a NaV-jarosite[18] consists of such ferromagnetic Kagomé planes which are coupled antiferromagnetically.

- We presented detailed spin-wave calculations for the most generic spin Hamiltonian allowed by symmetry. We derived analytic expressions for the spin-wave energies at the Γ, X, and Y points in the Brillouin zone. The agreement between our analytic and numerical results tends to support the correctness of both approaches. Since, the spectrum is invariant under a change of sign of D_y, the sign of this parameter remains undetermined by experiment.

- We obtained the spin-wave spectrum numerically throughout the Brillouin zone for a large number of models with increasing complexity and compared the results with the recent experimental data.[22] We obtained a nn exchange constant of $J_1 = 3.225$ meV, which is in good agreement with previous measurements.[22] We found that the observed small dispersion can be explained by a nnn isotropic interaction of $J_2 = 0.11$. The observed gaps at the Γ, X, and Y points are best explained by considering only the DM interaction with $|D_y| = 0.218$ meV and $D_z = -0.195$ meV together with nn and nnn interactions. The D_z term is adjusted to lift the zero-energy mode to about 8 meV with a small dispersion due to J_2 interaction. A fit of similar quality can also be obtained using the crystal field (CF) model of Ref. 16 but the resulting anisotropy is about 10% of J_1, too large a value for the S state Fe^{3+} ion which is supposed to be quite isotropic. The calculated canting angle is 2.07° and 0.77° for DM and CF models, respectively, compared to the experimentally deduced value[22] of 1.5°.

- Finally we discuss the effect of the canting on the spin-wave quantization axis which was neglected by Inami *et al.*[16] We found that neglecting canting is not a good approximation for calculating the spin-wave energy gaps at the high symmetry points in the Brillouin zone. When the CF is treated properly, it gives larger gaps at the Γ point than those from DM interaction. The experiment does not indicate significant splitting at the Γ point and therefore it suggests that the DM term works better to explain the data.

ACKNOWLEDGEMENT: We thank K. Matan and Y. S. Lee for many fruitful discussions and for sharing their spin-wave data prior to publication.

APPENDIX A: BOSON HAMILTONIAN

To construct the boson Hamiltonian it is convenient to introduce spherical components ($+ = x + iy$, $- = x - iy$) for interactions between site τ in unit cell i located at $\mathbf{R}_i$ and site τ' in unit cell j located at $\mathbf{R}_j$. If these sites are nth nearest neighbors, then we write

$$\begin{aligned}
\overline{\mathcal{I}}^{zz}_{\tau\tau'}(i,j) &= \overline{\mathcal{I}}^{(n)}_{zz} \ , \\
\overline{\mathcal{I}}^{\pm\pm}_{\tau\tau'}(i,j) &= \frac{1}{4}[\overline{\mathcal{I}}^{(n)}_{xx} - i\overline{\mathcal{I}}^{(n)}_{xy} - i\overline{\mathcal{I}}^{(n)}_{yx} - \overline{\mathcal{I}}^{(n)}_{yy}] \\
\overline{\mathcal{I}}^{\pm\mp}_{\tau\tau'}(i,j) &= \frac{1}{4}[\overline{\mathcal{I}}^{(n)}_{xx} \pm i\overline{\mathcal{I}}^{(n)}_{xy} \mp \overline{\mathcal{I}}^{(n)}_{yx} + \overline{\mathcal{I}}^{(n)}_{yy}]
\end{aligned} \tag{A1}$$

and similarly for the single-ion anisotropy matrix $\mathbf{C}$. Now we invoke the Holstein-Primakoff transformation in the form

$$S^z_{i\tau} = S - a^\dagger_{i\tau}a_{i\tau} \ , \ S^+_{i\tau} = \sqrt{2S}a_{i\tau} \ , \ S^-_{i\tau} = \sqrt{2S}a^\dagger_{i\tau} \tag{A2}$$

Then apart from a constant the Hamiltonian in terms of Bose operators is

$$\begin{aligned}
\mathcal{H} &= 2S\sum_{i\tau}\Big[-C^{zz}_\tau a^\dagger_{i\tau}a_{i\tau} + C^{++}_\tau a_{i\tau}a_{i\tau} + C^{--}_\tau a^\dagger_{i\tau}a^\dagger_{i\tau} \\
&\quad + C^{+-}_\tau a^\dagger_{i\tau}a_{i\tau} + C^{-+}_\tau a^\dagger_{i\tau}a_{i\tau}\Big] \\
&\quad + S\sum_{i\tau,j\tau'}{}' \Big[-\frac{1}{2}\overline{\mathcal{I}}^{zz}_{\tau\tau'}(i,j)(a^\dagger_{i\tau}a_{i\tau} + a^\dagger_{j\tau'}a_{j\tau'}) \\
&\quad + \overline{\mathcal{I}}^{++}_{\tau\tau'}(i,j)a_{i\tau}a_{j\tau'} + \overline{\mathcal{I}}^{--}_{\tau\tau'}(i,j)a^\dagger_{i\tau}a^\dagger_{j\tau'} \\
&\quad + \overline{\mathcal{I}}^{+-}_{\tau\tau'}(i,j)a_{i\tau}a^\dagger_{j\tau'} + \overline{\mathcal{I}}^{-+}_{\tau\tau'}(i,j)a^\dagger_{i\tau}a_{j\tau'}\Big] \ ,
\end{aligned} \tag{A3}$$

where the prime on the summation excludes the term with $(i,\tau) = (j,\tau')$. Now write

$$\begin{aligned}
a_{i\tau} &= \frac{1}{\sqrt{N}}\sum_{\mathbf{q}} e^{i\mathbf{q}\cdot(\mathbf{R}_i+\boldsymbol{\tau})}a_\tau(\mathbf{q}) \ , \\
a^\dagger_{i\tau} &= \frac{1}{\sqrt{N}}\sum_{\mathbf{q}} e^{-i\mathbf{q}\cdot(\mathbf{R}_i+\boldsymbol{\tau})}a^\dagger_\tau(\mathbf{q}) \ ,
\end{aligned} \tag{A4}$$

so that

$$\mathcal{H} = E_0 + \sum_{\mathbf{q}}\mathcal{H}(\mathbf{q}) \ , \tag{A5}$$

where E_0 is the ground state energy and

$$\mathcal{H}(\mathbf{q})/S = \sum_{\mu\nu} A_{\mu\nu}(\mathbf{q})a^\dagger_\mu(\mathbf{q})a_\nu(\mathbf{q})$$

$$+\frac{1}{2}\sum_{\alpha\beta} B_{\alpha\beta}(\mathbf{q}) a_\alpha^\dagger(\mathbf{q}) a_\beta^\dagger(-\mathbf{q})$$
$$+\frac{1}{2}\sum_{\alpha\beta} B_{\alpha\beta}(\mathbf{q})^* a_\alpha(\mathbf{q}) a_\beta(-\mathbf{q}) \ , \quad \text{(A6)}$$

where

$$\begin{aligned} A_{\tau,\tau'}(\mathbf{q}) &= \Big([2C_\tau^{+-} + 2C_\tau^{-+} - 2C_\tau^{zz} \\ &- \sum_{\tau''} \overline{\mathcal{I}}^{zz}_{\tau,\tau''}(q=0)]\delta_{\tau,\tau'} + \overline{\mathcal{I}}^{+-}_{\tau'\tau}(\mathbf{q}) + \overline{\mathcal{I}}^{-+}_{\tau\tau'}(-\mathbf{q}) \Big) \\ &= \Big([C_{xx} + \overline{C}_{yy} - 2\overline{C}_{zz} - \sum_{\tau''} \overline{\mathcal{I}}^{zz}_{\tau,\tau''}(q=0)]\delta_{\tau,\tau'} \\ &+ \overline{\mathcal{I}}^{+-}_{\tau'\tau}(\mathbf{q}) + \overline{\mathcal{I}}^{-+}_{\tau\tau'}(-\mathbf{q}) \Big) \end{aligned} \quad \text{(A7)}$$

$$\begin{aligned} B_{\tau,\tau'}(\mathbf{q}) &= 4C_\tau^{--}\delta_{\tau,\tau'} + 2\overline{\mathcal{I}}^{--}_{\tau\tau'}(-\mathbf{q}) \\ &= [C_{xx} - \overline{C}_{yy}]\delta_{\tau,\tau'} + 2\overline{\mathcal{I}}^{--}_{\tau\tau'}(-\mathbf{q}) \ , \end{aligned} \quad \text{(A8)}$$

where

$$\overline{\mathcal{I}}^{\alpha,\beta}_{\tau,\tau'}(\mathbf{q}) = \sum_i \overline{\mathcal{I}}^{\alpha,\beta}_{\tau,\tau'}(i,j) e^{i\mathbf{q}\cdot(\boldsymbol{\tau}+\mathbf{R}_{ij}-\boldsymbol{\tau}')} \ , \quad \text{(A9)}$$

where $\mathbf{R}_{ij} = \mathbf{R}_i - \mathbf{R}_j$ and the superscripts assume the values $+$, $-$, and z. Since each site is a center of inversion symmetry, the exponential factor in the sum over i in Eq. (A9) can be replaced by a cosine:

$$\overline{\mathcal{I}}^{\alpha,\beta}_{\tau,\tau'}(\mathbf{q}) = \sum_i \mathcal{I}^{\alpha,\beta}_{\tau,\tau'}(i,j) \cos[\mathbf{q}\cdot(\boldsymbol{\tau}+\mathbf{R}_{ij}-\boldsymbol{\tau}')] \quad \text{(A10)}$$

and $\overline{\mathcal{I}}(\mathbf{q})$ is an even function of $\mathbf{q}$. If $\mathbf{G}$ is a vector of the reciprocal lattice (such that $\mathbf{G}\cdot\mathbf{R}$ is a multiple of 2π), then

$$\begin{aligned} A_{\tau\tau'}(\mathbf{q}+\mathbf{G}) &= A_{\tau\tau'}(\mathbf{q}) e^{i\mathbf{G}\cdot(\boldsymbol{\tau}'-\boldsymbol{\tau})} \\ &= A_{\tau\tau'}(\mathbf{q}) \cos[\mathbf{G}\cdot(\boldsymbol{\tau}'-\tau)] \\ B_{\tau\tau'}(\mathbf{q}+\mathbf{G}) &= B_{\tau\tau'}(\mathbf{q}) e^{i\mathbf{G}\cdot(\boldsymbol{\tau}'-\boldsymbol{\tau})} \\ &= B_{\tau\tau'}(\mathbf{q}) \cos[\mathbf{G}\cdot(\boldsymbol{\tau}'-\tau)] \ . \end{aligned} \quad \text{(A11)}$$

Here we used the fact that for the Kagomé lattice, the $\boldsymbol{\tau}$'s are half a lattice vector, so that $e^{i\mathbf{G}\cdot(\boldsymbol{\tau}'-\boldsymbol{\tau})} = \cos[\mathbf{G}\cdot(\boldsymbol{\tau}'-\tau)] = \pm 1$.

APPENDIX B: NORMAL MODES

We write the normal mode operators as

$$X_\mu^\dagger(\mathbf{q}) = \sum_\alpha [c_\alpha^\mu(\mathbf{q}) a_\alpha^\dagger(\mathbf{q}) + d_\alpha^\mu(\mathbf{q}) a_\alpha(-\mathbf{q})] \ , \quad \text{(B1)}$$

and these are determined by

$$[\mathcal{H}, X_\mu^\dagger(\mathbf{q})] = \omega^{(\mu)}(\mathbf{q}) X_\mu^\dagger(\mathbf{q}) \ . \quad \text{(B2)}$$

If there are p spins per unit cell, then we expect that p of the $\omega^{(\mu)}$ will be nonnegative and p will be nonpositive.

Equation (B2) gives

$$\begin{aligned} &\tilde\omega^{(\mu)}(\mathbf{q}) \sum_\alpha [c_\alpha^\mu(\mathbf{q}) a_\alpha^\dagger(\mathbf{q}) + d_\alpha^\mu(\mathbf{q}) a_\alpha(-\mathbf{q})] \\ &= \sum_{\alpha,\beta} \Big[c_\alpha^\mu(\mathbf{q}) A_{\beta,\alpha}(\mathbf{q}) a_\beta^\dagger(\mathbf{q}) + c_\alpha^\mu(\mathbf{q}) B^*_{\alpha,\beta}(\mathbf{q}) a_\beta(-\mathbf{q}) \Big] \\ &\quad - \sum_{\alpha,\beta} \Big[d_\alpha^\mu(\mathbf{q}) A_{\alpha,\beta}(-\mathbf{q}) a_\beta(-\mathbf{q}) \\ &\quad + d_\alpha^\mu(\mathbf{q}) B_{\alpha,\beta}(-\mathbf{q}) a_\beta^\dagger(\mathbf{q}) \Big] \ , \end{aligned} \quad \text{(B3)}$$

where again $\tilde\omega \equiv \omega/S$.

1. Eigenvalue Problem

This leads to the eigenvalue problem

$$\begin{aligned} \tilde\omega^{(\mu)}(\mathbf{q}) c_\alpha^\mu(\mathbf{q}) &= \sum_\beta [A_{\alpha,\beta}(\mathbf{q}) c_\beta^\mu(\mathbf{q}) - B_{\beta,\alpha}(-\mathbf{q}) d_\beta^\mu(\mathbf{q})] \\ \tilde\omega^{(\mu)}(\mathbf{q}) d_\alpha^\mu(\mathbf{q}) &= \sum_\beta [B_{\beta,\alpha}(\mathbf{q})^* c_\beta^\mu(\mathbf{q}) - A_{\beta,\alpha}(-\mathbf{q}) d_\beta^\mu(\mathbf{q})] , \end{aligned} \quad \text{(B4)}$$

which can be written as

$$\begin{bmatrix} \mathbf{A}(\mathbf{q}) & -\tilde{\mathbf{B}}(-\mathbf{q}) \\ \tilde{\mathbf{B}}(\mathbf{q})^* & -\tilde{\mathbf{A}}(-\mathbf{q}) \end{bmatrix} \begin{bmatrix} \mathbf{c}^\mu(\mathbf{q}) \\ \mathbf{d}^\mu(\mathbf{q}) \end{bmatrix} = \tilde\omega^{(\mu)}(\mathbf{q}) \begin{bmatrix} \mathbf{c}^\mu(\mathbf{q}) \\ \mathbf{d}^\mu(\mathbf{q}) \end{bmatrix} , \quad \text{(B5)}$$

where $\mathbf{c}^\mu(\mathbf{q})$ is a column vector with components $c_1^\mu(\mathbf{q})$, $c_2^\mu(\mathbf{q})$, $\ldots$, $c_p^\mu(\mathbf{q})$, where $p=3$ is the number of spins in the unit cell.

We now note that because the Hamiltonian is Hermitian and taking account of inversion symmetry, we have

$$A_{\tau\tau'}(\mathbf{q}) = A_{\tau'\tau}(\mathbf{q})^* = A_{\tau\tau'}(-\mathbf{q}) \ . \quad \text{(B6)}$$

Similarly we write

$$B_{\tau\tau'}(\mathbf{q}) = B_{\tau'\tau}(-\mathbf{q}) = B_{\tau\tau'}(-\mathbf{q}) \ . \quad \text{(B7)}$$

Thus the eigenvalue problem is

$$\begin{bmatrix} \mathbf{A}(\mathbf{q}) & -\mathbf{B}(\mathbf{q}) \\ \mathbf{B}(\mathbf{q})^* & -\mathbf{A}(\mathbf{q})^* \end{bmatrix} \begin{bmatrix} \mathbf{c}^\mu(\mathbf{q}) \\ \mathbf{d}^\mu(\mathbf{q}) \end{bmatrix} = \tilde\omega^{(\mu)}(\mathbf{q}) \begin{bmatrix} \mathbf{c}^\mu(\mathbf{q}) \\ \mathbf{d}^\mu(\mathbf{q}) \end{bmatrix} \quad \text{(B8)}$$

We now show that the roots come in pairs with opposite signs. Equation (B8) is

$$\begin{aligned} \mathbf{A}\mathbf{c}^\mu - \mathbf{B}\mathbf{d}^\mu &= \tilde\omega^{(\mu)} \mathbf{c}^\mu \\ \mathbf{B}^*\mathbf{c}^\mu - \mathbf{A}^*\mathbf{d}^\mu &= \tilde\omega^{(\mu)} \mathbf{d}^\mu \ . \end{aligned} \quad \text{(B9)}$$

Take the complex conjugate of these equations, change the signs of both sides of each equations, and reorder the equations to get

$$\begin{aligned}\mathbf{A}[\mathbf{d}^\mu]^* - \mathbf{B}[\mathbf{c}^\mu]^* &= -\tilde{\omega}^{(\mu)}[\mathbf{d}^\mu]^* \\ \mathbf{B}^*[\mathbf{d}^\mu]^* - \mathbf{A}^*[\mathbf{c}^\mu]^* &= -\tilde{\omega}^{(\mu)}[\mathbf{c}^\mu]^* \ , \end{aligned} \quad (B10)$$

where we used the fact that the $\tilde{\omega}$'s are real. This shows that from an eigenvector with eigenvalue $\tilde{\omega}^{(\mu)}$ we can construct a related eigenvector with eigenvalue $-\tilde{\omega}^{(\mu)}$. One can show that the eigenvalues at wavevector $\mathbf{q}$ are identical to those at wavevector $-\mathbf{q}$, as expected in view of the inversion symmetry of the lattice. Thus we may write

$$\begin{aligned}&\left[\begin{array}{cc}\mathbf{A}(\mathbf{q}) & -\mathbf{B}(\mathbf{q}) \\ \mathbf{B}(\mathbf{q})^* & -\mathbf{A}(\mathbf{q})^*\end{array}\right]\left[\begin{array}{cc}\mathbf{c}(\mathbf{q}) & \mathbf{d}(\mathbf{q})^* \\ \mathbf{d}(\mathbf{q}) & \mathbf{c}(\mathbf{q})^*\end{array}\right] \\ &= \left[\begin{array}{cc}\mathbf{c}(\mathbf{q}) & \mathbf{d}(\mathbf{q})^* \\ \mathbf{d}(\mathbf{q}) & \mathbf{c}(\mathbf{q})^*\end{array}\right]\left[\begin{array}{cc}\tilde{\boldsymbol{\omega}}(\mathbf{q}) & 0 \\ 0 & -\tilde{\boldsymbol{\omega}}(\mathbf{q})\end{array}\right] \ , \end{aligned} \quad (B11)$$

where $\mathbf{c}(\mathbf{q})$ and $\mathbf{d}(\mathbf{q})$ are matrices whose columns are the column vectors $\mathbf{c}^\mu(\mathbf{q})$ and $\mathbf{d}^\mu(\mathbf{q})$, respectively, and $\tilde{\boldsymbol{\omega}}$ is a diagonal matrix with entries $\tilde{\omega}^{(\mu)}(\mathbf{q})$.

2. Dependence on Reciprocal Lattice Vector

Recall the dependence of the matrices on the reciprocal lattice vector as recorded in Eq. (A11). Then the eigenvalue problem at wavevector $\mathbf{q}+\mathbf{G}$ may be written in the form

$$\begin{aligned}&\tilde{\omega}^{(\mu)}(\mathbf{q}+\mathbf{G})c_\alpha^\mu(\mathbf{q}+\mathbf{G}) = \sum_\beta [A_{\alpha,\beta}(\mathbf{q})c_\beta^\mu(\mathbf{q}+\mathbf{G}) \\ &-B_{\beta,\alpha}(-\mathbf{q})d_\beta^\mu(\mathbf{q}+\mathbf{G})]e^{i\mathbf{G}\cdot(\boldsymbol{\tau}_\beta-\boldsymbol{\tau}_\alpha)} \\ &\tilde{\omega}^{(\mu)}(\mathbf{q}+\mathbf{G})d_\alpha^\mu(\mathbf{q}+\mathbf{G}) = \sum_\beta [B_{\beta,\alpha}(\mathbf{q})^* c_\beta^\mu(\mathbf{q}+\mathbf{G}) \\ &-A_{\beta,\alpha}(-\mathbf{q})d_\beta^\mu(\mathbf{q}+\mathbf{G})]e^{i\mathbf{G}\cdot(\boldsymbol{\tau}_\beta-\boldsymbol{\tau}_\alpha)} \ . \end{aligned} \quad (B12)$$

Set $\tilde{\omega}^{(\mu)}(\mathbf{q}+\mathbf{G}) = \tilde{\omega}^{(\mu)}(\mathbf{q})$ and

$$\begin{aligned}c_\beta^\mu(\mathbf{q}+\mathbf{G}) &= c_\beta^\mu(\mathbf{q})e^{-i\mathbf{G}\cdot\boldsymbol{\tau}_\beta} \\ d_\beta^\mu(\mathbf{q}+\mathbf{G}) &= d_\beta^\mu(\mathbf{q})e^{-i\mathbf{G}\cdot\boldsymbol{\tau}_\beta} \ . \end{aligned} \quad (B13)$$

Then we recover the previous equations. So we conclude that under addition of $\mathbf{G}$, the eigenvalues remain invariant, but the wavefunctions change according to Eq. (B13).

3. Orthogonality

Taking the Hermitian conjugate of eigenvalue equations, we get

$$\begin{aligned}\mathbf{c}^\mu(\mathbf{q})^\dagger\mathbf{A}(\mathbf{q}) - \mathbf{d}^\mu(\mathbf{q})^\dagger\mathbf{B}(\mathbf{q})^\dagger &= \tilde{\omega}^{(\mu)}(\mathbf{q})\mathbf{c}^\mu(\mathbf{q})^\dagger \\ \mathbf{c}^\mu(\mathbf{q})^\dagger\tilde{\mathbf{B}}(\mathbf{q}) - \mathbf{d}^\mu(\mathbf{q})^\dagger\tilde{\mathbf{A}}(\mathbf{q}) &= \tilde{\omega}^{(\mu)}(\mathbf{q})\mathbf{d}^\mu(\mathbf{q})^\dagger \end{aligned} \quad (B14)$$

so that

$$\begin{aligned}&\left[\begin{array}{cc}\mathbf{c}^\mu(\mathbf{q})^\dagger \ , & -\mathbf{d}^\mu(\mathbf{q})^\dagger\end{array}\right]\left[\begin{array}{cc}\mathbf{A}(\mathbf{q}) & -\mathbf{B}(\mathbf{q}) \\ \mathbf{B}(\mathbf{q})^* & -\mathbf{A}(\mathbf{q})^*\end{array}\right] \\ &= \tilde{\omega}^{(\mu)}(\mathbf{q})\left[\begin{array}{cc}\mathbf{c}^\mu(\mathbf{q})^\dagger \ , & -\mathbf{d}^\mu(\mathbf{q})^\dagger\end{array}\right] \ . \end{aligned} \quad (B15)$$

Thus from any right solution we have constructed the associated left solution. Now consider

$$\begin{aligned}W_{\mu\nu} &\equiv \left[c^\mu(\mathbf{q})^\dagger \ , -d^\mu(\mathbf{q})^\dagger\right]\left[\begin{array}{cc}\mathbf{A}(\mathbf{q}) & -\mathbf{B}(\mathbf{q}) \\ \mathbf{B}(\mathbf{q})^* & -\mathbf{A}(\mathbf{q})^*\end{array}\right] \\ &\times\left[\begin{array}{c}c^\nu(\mathbf{q}) \\ d^\nu(\mathbf{q})\end{array}\right] \ . \end{aligned} \quad (B16)$$

Using the fact that the left and right vectors are eigenvectors, we have

$$\begin{aligned}W_{\mu\nu} &= \tilde{\omega}^{(\mu)}(\mathbf{q})^*\left[\begin{array}{cc}\mathbf{c}^\mu(\mathbf{q})^\dagger \ , & -\mathbf{d}^\mu(\mathbf{q})^\dagger\end{array}\right]\left[\begin{array}{c}c^\nu(\mathbf{q}) \\ d^\nu(\mathbf{q})\end{array}\right] \\ &= \tilde{\omega}^{(\nu)}(\mathbf{q})\left[\begin{array}{cc}\mathbf{c}^\mu(\mathbf{q})^\dagger \ , & -\mathbf{d}^\mu(\mathbf{q})^\dagger\end{array}\right]\left[\begin{array}{c}c^\nu(\mathbf{q}) \\ d^\nu(\mathbf{q})\end{array}\right] \end{aligned} \quad (B17)$$

If $\mu=\nu$ this shows that $\tilde{\omega}^{(\mu)}(\mathbf{q})$ is real. Also

$$\left[\begin{array}{cc}\mathbf{c}^\mu(\mathbf{q})^\dagger \ , & -\mathbf{d}^\mu(\mathbf{q})^\dagger\end{array}\right]\left[\begin{array}{c}c^\nu(\mathbf{q}) \\ d^\nu(\mathbf{q})\end{array}\right] = 0, \quad \mu \neq \nu \ . \quad (B18)$$

(If we have degenerate eigenvalues, we can choose the wavefunctions to preserve this orthogonality.)

A more general orthogonality is

$$\left[\begin{array}{cc}\mathbf{c}^\dagger(\mathbf{q}) & -\mathbf{d}^\dagger(\mathbf{q}) \\ -\tilde{\mathbf{d}}(\mathbf{q}) & \tilde{\mathbf{c}}(\mathbf{q})\end{array}\right]\left[\begin{array}{cc}\mathbf{c}(\mathbf{q}) & \mathbf{d}(\mathbf{q})^* \\ \mathbf{d}(\mathbf{q}) & \mathbf{c}(\mathbf{q})^*\end{array}\right] = \mathcal{I} \ , \quad (B19)$$

where $\mathcal{I}$ is the $2p \times 2p$ unit matrix.

4. Summary

We have the transformation to normal modes as

$$X_\mu^\dagger(\mathbf{q}) = \sum_\alpha [c_\alpha^\mu(\mathbf{q})a_\alpha^\dagger(\mathbf{q}) + d_\alpha^\mu(\mathbf{q})a_\alpha(-\mathbf{q})] \ , \quad (B20)$$

and also

$$X_\mu(\mathbf{q}) = \sum_\alpha [c_\alpha^\mu(\mathbf{q})^* a_\alpha(\mathbf{q}) + d_\alpha^\mu(\mathbf{q})^* a_\alpha^\dagger(-\mathbf{q})] \ , \quad (B21)$$

where μ is restricted so that $\tilde{\omega}^{(\mu)} > 0$. We require that $X_\mu(\mathbf{q})$ obey Bose commutation relations:

$$[X_\mu(\mathbf{q}), X_\nu^\dagger(\mathbf{q})] = \delta_{\mu,\nu} \ . \quad (B22)$$

This gives

$$\sum_\tau \left(c_\tau^\mu(\mathbf{q})^* c_\tau^\nu(\mathbf{q}) - d_\tau^\mu(\mathbf{q})^* d_\tau^\nu(\mathbf{q})\right) = \delta_{\mu,\nu} \ . \quad (B23)$$

The inverse transformation is

$$a_\alpha^\dagger(\mathbf{q}) = \sum_\mu [c_\alpha^\mu(\mathbf{q})^* X_\mu(\mathbf{q})^\dagger - d_\alpha^\mu(\mathbf{q}) X_\mu(-\mathbf{q})] ,$$
$$a_\alpha(\mathbf{q}) = \sum_\mu [c_\alpha^\mu(\mathbf{q}) X_\mu(\mathbf{q}) - d_\alpha^\mu(\mathbf{q})^* X_\mu(-\mathbf{q})^\dagger] \quad \text{(B24)}$$

We record here the dependence on reciprocal lattice vector:

$$a_\alpha^\dagger(\mathbf{q}+\mathbf{G}) = \sum_\mu [c_\alpha^\mu(\mathbf{q})^* X_\mu(\mathbf{q})^\dagger - d_\alpha^\mu(\mathbf{q}) X_\mu(-\mathbf{q})] e^{i\mathbf{G}\cdot\boldsymbol{\tau}_\alpha} ,$$
$$a_\alpha(\mathbf{q}+\mathbf{G}) = \sum_\mu [c_\alpha^\mu(\mathbf{q}) X_\mu(\mathbf{q}) - d_\alpha^\mu(\mathbf{q})^* X_\mu(-\mathbf{q})^\dagger] e^{-i\mathbf{G}\cdot\boldsymbol{\tau}_\alpha} \quad \text{(B25)}$$

To use this we would assume that $\mathbf{q}$ is in the first Brillouin zone and $\mathbf{G}$ is the vector needed to bring the actual wavevector back into the first Brillouin zone.

APPENDIX C: EXPLICIT EVALUATION OF MATRIX ELEMENTS

We now develop explicit expressions for the constants appearing in these matrices. We use Eq. (35) to relate the overlined coefficients to the bare coefficients, which are defined in Eqs. (33) and (24). We will work to second order in the perturbations from isotropic exchange. To this order

$$\sin(2\theta) = \frac{H_y}{H} = \frac{H_y}{H_z} \quad \text{(C1)}$$

and

$$\cos(2\theta) = \frac{H_z}{\sqrt{H_z^2 + H_y^2}} = 1 - \frac{H_y^2}{2H_z^2} , \quad \text{(C2)}$$

where H_y and H_z are given in Eq. (31), so that

$$\sin(2\theta) = \left(\frac{2}{3J_1}\right) \frac{J_{yz} - C_{yz} - \sqrt{3}D_y}{\left[1 + \frac{Z}{J_1}\right]} , \quad \text{(C3)}$$

where

$$Z = J_2 + \frac{\Delta_J}{4} - \frac{\eta_J}{12} - \frac{\sqrt{3}D_z}{3} + \frac{C_{y-z}}{3} . \quad \text{(C4)}$$

Then

$$\cos(2\theta) = 1 - \frac{2}{9J_1^2}(J_{yz} - C_{yz} - \sqrt{3}D_y)^2 . \quad \text{(C5)}$$

Equation (35) gives

$$\begin{aligned}\overline{\Delta} &\equiv C_{xx} + \overline{C}_{yy} = C_{xx} + C_{yy} - 2C_{zz} - 3C_{yz}\sin(2\theta) \\ &= \Delta - 3C_{yz}\sin(2\theta) . \end{aligned} \quad \text{(C6)}$$

Then, keeping only relevant anisotropy corrections, we find that the constants in Eq. (43) and (44) are

$$\begin{aligned}
A_0 &= 4\overline{E}_z^{(1)} + \overline{\Delta} \\
&= \Delta + 2E_z^{(1)} + 2E_y^{(1)} + [2E_z^{(1)} - 2E_y^{(1)}]\cos(2\theta) \\
&\quad -[4E_{yz}^{(1)} + 3C_{yz}]\sin(2\theta) \\
&= \Delta + \frac{3}{2}J_{xx} - \frac{1}{2}J_{yy} - 2J_{zz} - \sqrt{3}D_z \\
&\quad + \left[\frac{3}{2}J_{xx} - \frac{1}{2}J_{yy} + 2J_{zz} - \sqrt{3}D_z\right] \\
&\quad \times \left[1 - \frac{2[J_{yz} - C_{yz} - \sqrt{3}D_y]^2}{9J_1^2}\right] \\
&\quad - \frac{1}{3J_1}\left[4\sqrt{3}D_y - 4J_{yz} + 6C_{yz}\right]\left[J_{yz} - C_{yz} - \sqrt{3}D_y\right] \\
&= 2J + \Delta + \frac{5}{6}\Delta_J + \frac{3}{2}\eta_J - 2\sqrt{3}D_z \\
&\quad + \frac{2}{3J_1}[J_{yz} - C_{yz} - \sqrt{3}D_y][J_{yz} - \sqrt{3}D_y - 2C_{yz}] ,
\end{aligned}$$

$$\begin{aligned}
A_1 &= -E_x^{(1)} - \overline{E}_y^{(1)} \\
&= -E_x^{(1)} - [E_z^{(1)} + E_y^{(1)}]/2 \\
&\quad - \frac{1}{2}[E_y^{(1)} - E_z^{(1)}]\cos(2\theta) - E_{yz}^{(1)}\sin(2\theta) \\
&= \frac{1}{4}J_{xx} - \frac{3}{4}J_{yy} + \frac{\sqrt{3}}{2}D_z - \frac{3}{8}J_{xx} \\
&\quad + \frac{1}{8}J_{yy} + \frac{1}{2}J_{zz} + \frac{\sqrt{3}}{4}D_z \\
&\quad + \left[\frac{1}{2}J_{zz} + \frac{3}{8}J_{xx} - \frac{1}{8}J_{yy} - \frac{\sqrt{3}}{4}D_z\right] \\
&\quad \times \left[1 - \frac{2[J_{yz} - C_{yz} - \sqrt{3}D_y]^2}{9J_1^2}\right] \\
&\quad - \frac{1}{3J_1}[\sqrt{3}D_y - J_{yz}][J_{yz} - C_{yz} - \sqrt{3}D_y] \\
&= \frac{1}{2}J_1 - \frac{3}{8}\eta_J + \frac{11}{24}\Delta_J + \frac{\sqrt{3}}{2}D_z \\
&\quad + \frac{1}{6J_1}\left[J_{yz} - C_{yz} - \sqrt{3}D_y\right]\left[-\sqrt{3}D_y + J_{yz} + C_{yz}\right] ,
\end{aligned}$$

$$\begin{aligned}
B_0 &= C_{xx} - \overline{C}_{yy} , \\
&= C_{xx} - \frac{1}{2}\left[C_{yy} + C_{zz}\right] + \frac{1}{2}\left[C_{zz} - C_{yy}\right]\cos(2\theta) \\
&\quad + C_{yz}\sin(2\theta) \\
&= C_{xx} - C_{yy} + \frac{2C_{yz}}{3J_1}[J_{yz} - C_{yz} - \sqrt{3}D_y] ,
\end{aligned}$$

$$\begin{aligned}
B_1 &= -E_x^{(1)} + \overline{E}_y^{(1)} \\
&= -E_x^{(1)} + \frac{1}{2}\left[E_y^{(1)} + E_z^{(1)}\right] + E_{yz}^{(1)}\sin(2\theta)
\end{aligned}$$

$$
\begin{aligned}
& +\frac{1}{2}\left[E_y^{(1)} - E_z^{(1)}\right]\cos(2\theta) \\
= & \ \frac{5}{8}J_{xx} - \frac{7}{8}J_{yy} - \frac{1}{2}J_{zz} + \frac{\sqrt{3}}{4}D_z \\
& -\frac{1}{2}\left[J_{zz} + \frac{3}{4}J_{xx} - \frac{1}{4}J_{yy} - \frac{\sqrt{3}}{2}D_z\right] \\
& \times\left[1 - \frac{2[J_{yz} - C_{yz} - \sqrt{3}D_y]^2}{9J_1^2}\right] \\
& +\frac{1}{3J_1}[\sqrt{3}D_y - J_{yz}][J_{yz} - C_{yz} - \sqrt{3}D_y] \\
= & \ -\frac{3}{2}J_1 + \frac{5}{8}\eta_J + \frac{1}{8}\Delta_J + \frac{\sqrt{3}}{2}D_z \\
& +\frac{[J_{yz} - C_{yz} - \sqrt{3}D_y]}{6J}[\sqrt{3}D_y - J_{yz} - C_{yz}] \ , \\
\alpha^{(1)} = & \ 2\overline{d}_z^{(1)} = 2d_z^{(1)}\cos\theta + 2d_y^{(1)}\sin\theta \\
= & \ 2d_z^{(1)} + d_y^{(1)}\sin(2\theta) \\
= & \ -(D_y + \sqrt{3}J_{yz})\cos\theta \\
+ & \left(-\sqrt{3}J_1 - D_z + \frac{\sqrt{3}\Delta_J}{12} - \frac{\sqrt{3}\eta_J}{4}\right)\sin\theta \ . \qquad \text{(C7)}
\end{aligned}
$$

But using Eq. (C3) this gives

$$
\begin{aligned}
\alpha^{(1)} = & \ -D_y - \sqrt{3}J_{yz} + \frac{J_{yz} - C_{yz} - \sqrt{3}D_y}{3J_1} \\
& \times\left[1 - \frac{Z}{J_1}\right]\left[-\sqrt{3}J_1 - D_z + \frac{\sqrt{3}\Delta_J}{12} - \frac{\sqrt{3}\eta_J}{4}\right] \\
= & \ -\frac{4\sqrt{3}}{3}J_{yz} + \frac{C_{yz}}{\sqrt{3}} + \frac{J_{yz} - C_{yz} - \sqrt{3}D_y}{3\sqrt{3}J_1} \\
& \times\left[\Delta_J - \eta_J - 2\sqrt{3}D_z + C_{y-x} + 3J_2\right] \ . \qquad \text{(C8)}
\end{aligned}
$$

Also

$$
\begin{aligned}
\alpha^{(2)} = & \ 2d_z^{(2)}\cos\theta + 2d_y^{(2)}\sin\theta \\
= & \ (-\sqrt{3}J_2)\sin\theta \\
= & \ -\frac{\sqrt{3}J_2}{3J_1}\left[J_{yz} - C_{yz} - \sqrt{3}D_y\right] \ . \qquad \text{(C9)}
\end{aligned}
$$

APPENDIX D: DYNAMICAL STRUCTURE FACTOR

We first define the Green's function

$$
\begin{aligned}
\langle\langle A;B\rangle\rangle_\omega = & \sum_n p_n\left[\frac{\langle n|A|m\rangle\langle m|B|n\rangle}{\omega - E_m + E_n}\right. \\
& \left. - \frac{\langle n|B|m\rangle\langle m|A|n\rangle}{\omega + E_m - E_n}\right] \ . \qquad \text{(D1)}
\end{aligned}
$$

Then we will need the frequency and wave vector dependent susceptibility given by

$$
\chi^{\alpha\beta}(\omega,\mathbf{q}) = \langle\langle\mathcal{S}^\alpha(\mathbf{q});\mathcal{S}^\beta(-\mathbf{q})\rangle\rangle_\omega \qquad \text{(D2)}
$$

in terms of which the dynamical structure factor is

$$
\mathcal{S}(\omega,\mathbf{q}) = \frac{n(\omega)}{\pi}\sum_{\alpha\beta}\Im\chi^{\alpha\beta}(\omega - i0^+,\mathbf{q})[\delta_{\alpha,\beta} - \hat{q}_\alpha\hat{q}_\beta] , \qquad \text{(D3)}
$$

where $n(\omega) = [e^{\beta\omega} - 1]^{-1}$. We have that

$$
\begin{aligned}
& \frac{n(\omega)}{\pi}\Im\chi^{\alpha\beta}(\omega - i0^+,\mathbf{q}) \\
& = \sum_{m,n} p_n\Big[\delta(\omega - E_m + E_n)\langle n|\mathcal{S}^\alpha(\mathbf{q})|m\rangle\langle m|\mathcal{S}^\beta(-\mathbf{q})|n\rangle \\
& \quad -\delta(\omega + E_m - E_n)\langle n|\mathcal{S}^\beta(-\mathbf{q})|m\rangle\langle m|\mathcal{S}^\alpha(\mathbf{q})|n\rangle\Big] n(\omega) \\
= & \sum_{m,n}\Big\{p_n\delta(\omega - E_m + E_n)\langle n|\mathcal{S}^\alpha(\mathbf{q})|m\rangle\langle m|\mathcal{S}^\beta(-\mathbf{q})|n\rangle \\
& \quad -p_m\delta(\omega + E_n - E_m)\langle m|\mathcal{S}^\beta(-\mathbf{q})|n\rangle\langle n|\mathcal{S}^\alpha(\mathbf{q})|m\rangle\Big\} n(\omega) \\
= & \sum_{m,n} p_n\delta(\omega - E_m + E_n)[1 - e^{-\beta(E_m - E_n)}]n(\omega) \\
& \quad \times\langle n|\mathcal{S}^\alpha(\mathbf{q})|m\rangle\langle m|\mathcal{S}^\beta(-\mathbf{q})|n\rangle \\
= & \sum_{m,n} p_n\delta(\omega - E_m + E_n)\frac{1 - e^{-\beta(E_m - E_n)}]}{e^{\beta(E_m - E_n)} - 1} \\
& \quad \times\langle n|\mathcal{S}^\alpha(\mathbf{q})|m\rangle\langle m|\mathcal{S}^\beta(-\mathbf{q})|n\rangle \\
= & \sum_{m,n} p_m\delta(\omega - E_m + E_n)\langle n|\mathcal{S}^\alpha(\mathbf{q})|m\rangle\langle m|\mathcal{S}^\beta(-\mathbf{q})|n\rangle \ . \qquad \text{(D4)}
\end{aligned}
$$

We write

$$
\begin{aligned}
\mathcal{S}^\alpha(\mathbf{q}) = & \ \frac{1}{\sqrt{N}}\sum_i e^{i\mathbf{q}\cdot\mathbf{r}_i}\mathcal{S}^\alpha(i) \\
= & \ \frac{1}{\sqrt{N}}\sum_{\boldsymbol{\tau},\mathbf{R}} e^{i\mathbf{q}\cdot(\boldsymbol{\tau}+\mathbf{R})}\mathcal{S}^\alpha(\mathbf{R},\boldsymbol{\tau}) \\
= & \ \frac{1}{\sqrt{N}}\sum_{\boldsymbol{\tau},\mathbf{R},\rho} e^{i\mathbf{q}\cdot(\boldsymbol{\tau}+\mathbf{R})}\mathcal{R}_{\alpha\rho}(\tau)S_\ell^\rho(\mathbf{R},\boldsymbol{\tau}) \ , \qquad \text{(D5)}
\end{aligned}
$$

where the subscript ℓ indicates a component with respect to the local canted axes. Then, to linear order in the Bose operators we have

$$
\begin{aligned}
\mathcal{S}^\alpha(\mathbf{q}) = & \ \frac{1}{\sqrt{N}}\sum_{\boldsymbol{\tau},\mathbf{R}} e^{i\mathbf{q}\cdot(\boldsymbol{\tau}+\mathbf{R})} \\
& \times\left[\mathcal{R}_{\alpha x}(\tau)S_\ell^x(\mathbf{R},\boldsymbol{\tau}) + \mathcal{R}_{\alpha y}(\tau)S_\ell^y(\mathbf{R},\boldsymbol{\tau})\right] \\
= & \ \sqrt{\frac{S}{2N}}\sum_{\boldsymbol{\tau},\mathbf{R}} e^{i\mathbf{q}\cdot(\boldsymbol{\tau}+\mathbf{R})}
\end{aligned}
$$

$$\times\Bigg(\mathcal{R}_{\alpha x}(\tau)[a(\mathbf{R},\boldsymbol{\tau})+a^\dagger(\mathbf{R},\boldsymbol{\tau})]$$
$$-i\mathcal{R}_{\alpha y}(\tau)[a(\mathbf{R},\boldsymbol{\tau})-a^\dagger(\mathbf{R},\boldsymbol{\tau})]\Bigg)\ . \qquad \text{(D6)}$$

Now set

$$\Gamma_\alpha(\tau)\ \equiv\ \mathcal{R}_{\alpha x}(\tau)+i\mathcal{R}_{\alpha y}(\tau)\ . \qquad \text{(D7)}$$

Then

$$\begin{aligned}
\mathcal{S}^\alpha(\mathbf{q}) &= \sqrt{\frac{S}{2N}}\sum_{\mathbf{R}\boldsymbol{\tau}} e^{i\mathbf{q}\cdot(\mathbf{R}+\boldsymbol{\tau})}\left[\Gamma_\alpha(\tau)a^\dagger(\mathbf{R}\tau)+\Gamma_\alpha(\tau)^*a(\mathbf{R}\tau)\right]\\
&= \sqrt{\frac{S}{2}}\sum_{\boldsymbol{\tau}}\left[\Gamma_\alpha(\tau)a_\tau^\dagger(\mathbf{q})+\Gamma_\alpha(\tau)^*a_\tau(-\mathbf{q})\right]\\
&= \sqrt{\frac{S}{2}}\sum_{\boldsymbol{\tau}\mu}\Bigg[\Gamma_\alpha(\tau)\left(c_\tau^{(\mu)}(\mathbf{q})^*X_\mu^\dagger(\mathbf{q})-d_\tau^{(\mu)}(\mathbf{q})X_\mu(-\mathbf{q})\right)\\
&\quad +\Gamma_\alpha(\tau)^*\left(c_\tau^{(\mu)}(-\mathbf{q})X_\mu(-\mathbf{q})-d_\tau^{(\mu)}(-\mathbf{q})^*X_\mu^\dagger(\mathbf{q})\right)\Bigg]\\
&= \sqrt{\frac{S}{2}}\sum_{\boldsymbol{\tau}\mu}\Bigg[\left(\Gamma_\alpha(\tau)c_\tau^{(\mu)}(\mathbf{q})^*-\Gamma_\alpha(\tau)^*d_\tau^{(\mu)}(\mathbf{q})^*\right)X_\mu^\dagger(\mathbf{q})\\
&\quad +\left(\Gamma_\alpha(\tau)^*c_\tau^{(\mu)}(\mathbf{q})-\Gamma_\alpha(\tau)d_\tau^{(\mu)}(\mathbf{q})\right)X_\mu(-\mathbf{q})\Bigg]\ . \qquad \text{(D8)}
\end{aligned}$$

For general reciprocal lattice vector one has

$$\begin{aligned}
&\mathcal{S}^\alpha(\mathbf{q}+\mathbf{G})=\sqrt{S/2}\\
&\times\sum_{\boldsymbol{\tau}\mu}\Bigg[\left(\Gamma_\alpha(\tau)c_\tau^{(\mu)}(\mathbf{q})^*-\Gamma_\alpha(\tau)^*d_\tau^{(\mu)}(\mathbf{q})^*\right)X_\mu^\dagger(\mathbf{q})\\
&+\left(\Gamma_\alpha(\tau)^*c_\tau^{(\mu)}(\mathbf{q})-\Gamma_\alpha(\tau)d_\tau^{(\mu)}(\mathbf{q})\right)X_\mu(-\mathbf{q})\Bigg]e^{i\mathbf{G}\cdot\boldsymbol{\tau}} \qquad \text{(D9)}
\end{aligned}$$

This result indicates that the scattering intensity will oscillate when $e^{i\mathbf{G}\cdot\boldsymbol{\tau}}$ changes sign as one goes from one Brillouin zone to the next.

[1] G. Misguich and C. Lhuillier, *Frustrated Spin Systems*, edited by H. T. Diep (World Scientific, Singapore, 2004), and references therein.
[2] A. P. Ramirez, in *Handbook on Magnetic Materials* (ed. K. J. H. Busch), **Vol. 13**, 423 (Elsevier Science, Amsterdam, 2001).
[3] S. Sachdev, Phys. Rev. B **45**, 12377 (1992).
[4] D. A. Huse and A. D. Rutenberg, Phys. Rev. B **45**, 7536 (1992).
[5] A. B. Harris, C. Kallin, and A. J. Berlinsky, Phys. Rev. B **45**, 2899 (1992).
[6] F. Mila, Phys. Rev. Lett. **81**, 2356 (1998).
[7] P. Sindzingre, G. Misguich, C. Lhuillier, B. Bernu, L. Pierre, Ch. Waldtmann, and H.-U. Evert, Phys. Rev. Lett. **84**, 2953 (2000).
[8] F. Bert, D. Bono, P. Mendels, F. Ladieu, F. Duc, J.-C. Trombe, and P. Millet, Phys. Rev. Lett. **95**, 087203 (2005).
[9] E. F. Shender, P. C. W. Holdsworth in *Fluctuations and Order*, p. 259, edited by M. Millonas (Springer, Berlin, 1996).
[10] T. Yildirim, Tr. J. of Physics, **23**, 47 (1999).
[11] S. H. Lee, C. Broholm, G. Aeppli, T. G. Perring, B. Hessen, and A. Taylor, Phys. Rev. Lett. **76**, 4424 (1996).
[12] A. Keren, Y. J. Uemura, G. Luke, P. Mendels, M. Mekata, T. Asano, Phys. Rev. Lett. **84**, 3450 (2000).
[13] M. G. Townsend, G. Longworth, and E. Roudaut, Phys. Rev. B **33**, 4919 (1986).
[14] T. Inami, M. Nishiyama, S. Maegawa, and Y. Oka, Phys. Rev. B **61**, 12181 (2000).
[15] A. S. Wills, Phys. Rev. B **63**, 064430 (2001).
[16] M. Nishiyama, S. Maegawa, T. Inami, and Y. Oka, Phys. Rev. B **67**, 224435 (2003).
[17] D. Grohol, D. G. Nocera, and D. Papoutsakis, Phsy. Rev. B **67**, 064401 (2003).
[18] D. Grohol, Q. Huang, B. H. Toby, J. W. Lynn, Y. S. Lee, and D. G. Nocera, Phys. Rev. B **68**, 094404 (2003)
[19] B. M. Bartlett and D. G. Nocera, J. Am. Chem. Soc. **127**, 8985 (2005).
[20] M. Elhajal, B. Canals, and C. Lacroix, Phys. Rev. B **66**, 014422 (2002).
[21] D. Grohol, K. Matan, J. H. Cho, S. H. Lee, J. W. Lynn, D. G. Nocera, and Y. S. Lee, Nature Materials **4**, 323 (2005).
[22] K. Matan, D. Grohol, D. G. Nocera, T. Yildirim, A. B. Harris, S.-H. Lee, S. E. Nagler, and Y. S. Lee, arXiv:cond-mat/0602036 (3 Feb. 2006).
[23] I. E. Dzyaloshinskii, J. Phys. Chem. Solids **4**, 241 (1958).
[24] T. Moriya, Phys. Rev. **120**, 91 (1960).
[25] *International Tables for Crystallography*, (D. Riedel, Boston, 1993), Ed. T. Hahn, Vol. A.
[26] E. P. Wigner, *Group Theory*, (Academic, New York, 1959). M. Tinkham, Group Theory and Quantum Mechanics, (McGraw-Hill, New York, 1964).
[27] T. Thio *et al.*, Phys. Rev. B **38**, 905 (1988).